

PAPER • OPEN ACCESS

Electrical spiking activity of proteinoids-ZnO colloids

To cite this article: Panagiotis Mougkogiannis *et al* 2024 *Neuromorph. Comput. Eng.* 4 014007

View the [article online](#) for updates and enhancements.

You may also like

- [ENANTIOMERIC EXCESSES INDUCED IN AMINO ACIDS BY ULTRAVIOLET CIRCULARLY POLARIZED LIGHT IRRADIATION OF EXTRATERRESTRIAL ICE ANALOGS: A POSSIBLE SOURCE OF ASYMMETRY FOR PREBIOTIC CHEMISTRY](#)

Paola Modica, Cornelia Meinert, Pierre de Marcellus *et al.*

- [NATURE'S STARSHIPS. I. OBSERVED ABUNDANCES AND RELATIVE FREQUENCIES OF AMINO ACIDS IN METEORITES](#)

Alyssa K. Cobb and Ralph E. Pudritz

- [NATURE'S STARSHIPS. II. SIMULATING THE SYNTHESIS OF AMINO ACIDS IN METEORITE PARENT BODIES](#)



Alyssa K. Cobb, Ralph E. Pudritz and Ben K. D. Pearce



PAPER

Electrical spiking activity of proteinoids-ZnO colloids

OPEN ACCESS

Panagiotis Mougkogiannis^{1,*} , Noushin Raeisi Kheirabadi¹, Alessandro Chiolerio^{1,2} 
and Andrew Adamatzky¹RECEIVED
4 July 2023REVISED
4 January 2024ACCEPTED FOR PUBLICATION
20 February 2024PUBLISHED
1 March 2024Original Content from
this work may be used
under the terms of the
[Creative Commons
Attribution 4.0 licence](#).Any further distribution
of this work must
maintain attribution to
the author(s) and the title
of the work, journal
citation and DOI.¹ Unconventional Computing Laboratory, UWE, Bristol, United Kingdom² Center for Bioinspired Soft Robotics, Istituto Italiano di Tecnologia, Genova, Italy

* Author to whom any correspondence should be addressed.

E-mail: Panagiotis.Mougkogiannis@uwe.ac.uk**Keywords:** thermal proteins, proteinoids, microspheres, electrical activity, neuromorphic architectures, unconventional computing, liquid roboticsSupplementary material for this article is available [online](#)**Abstract**

We are studying the remarkable electrical properties of Proteinoids-ZnO microspheres with the aim of exploring their potential for a new form of computing. Our research has revealed that these microspheres exhibit behavior similar to neurons, generating electrical spikes that resemble action potentials. Through our investigations, we have studied the underlying mechanism behind this electrical activity and proposed that the spikes arise from oscillations between the degradation and reorganization of proteinoid molecules on the surface of ZnO. These findings offer valuable insights into the potential use of Proteinoids-ZnO colloids in unconventional computing and the development of novel neuromorphic liquid circuits.

1. Introduction

Thermal proteins (proteinoids) [1] are produced by heating amino acids to their melting point and initiating polymerization to produce polymeric chains. The polymerization happens at 160 °C–200 °C, in the absence of a solvent, an initiator, or a catalyst, in an inert atmosphere. The tri-functional amino acids, e.g. glutamic acid or aspartic acid or lysine, undergo cyclization at high temperatures and become solvents and initiators of polymerization for other amino acids [1, 2]. It is possible to produce proteinoids that are either acidic or basic via this simple thermal condensation reaction. A proteinoid can be swollen in an aqueous solution at moderate temperatures (approximately 50 °C) forming a structure known as a microsphere [1]. The microspheres are hollow, usually filled with an aqueous solution. Proteinoids possess distinct chemical and physical features [3–5] that can generate electrical spiking behaviour in diverse nanoscale composites. The proteinoids are sufficiently accurate prototypes of terrestrial protocells with bioelectrical properties [6, 7]. Having most characteristics of excitable cells, proteinoid microspheres have been considered as protoneurons [8]. A consensus was achieved that proteinoids directly led into neurons, which then self-associated into brains [1] (figure 1).

Proteinoids, which are synthetic amino acids, have been effectively utilised in various materials including nanofibers, optical waveguides, and nanosensors [10–12]. On the other hand, ZnO colloids have already shown interesting features, among which: resistive switching features [13–16], their potential to function as electrical-analogue neurons [17], and the manifestation of Pavlovian reflexes [18].

Proteinoid-ZnO colloid hybrids exhibit potential for controllable electrical spiking behaviour under various external stimuli. Research has indicated that modifications in surface potential, surface chemistry, and material composition can considerably impact the electrical spiking of proteinoid-ZnO colloids [19–21]. The electrical spiking behaviour of the proteinoid-ZnO colloid hybrid can be adjusted by modifying its chemical or surface properties.

Colloid mixtures, such as proteinoids-ZnO colloid hybrids, have the potential to generate novel prototypes of distributed information processing devices [22–24]. To comprehend the potential of these new

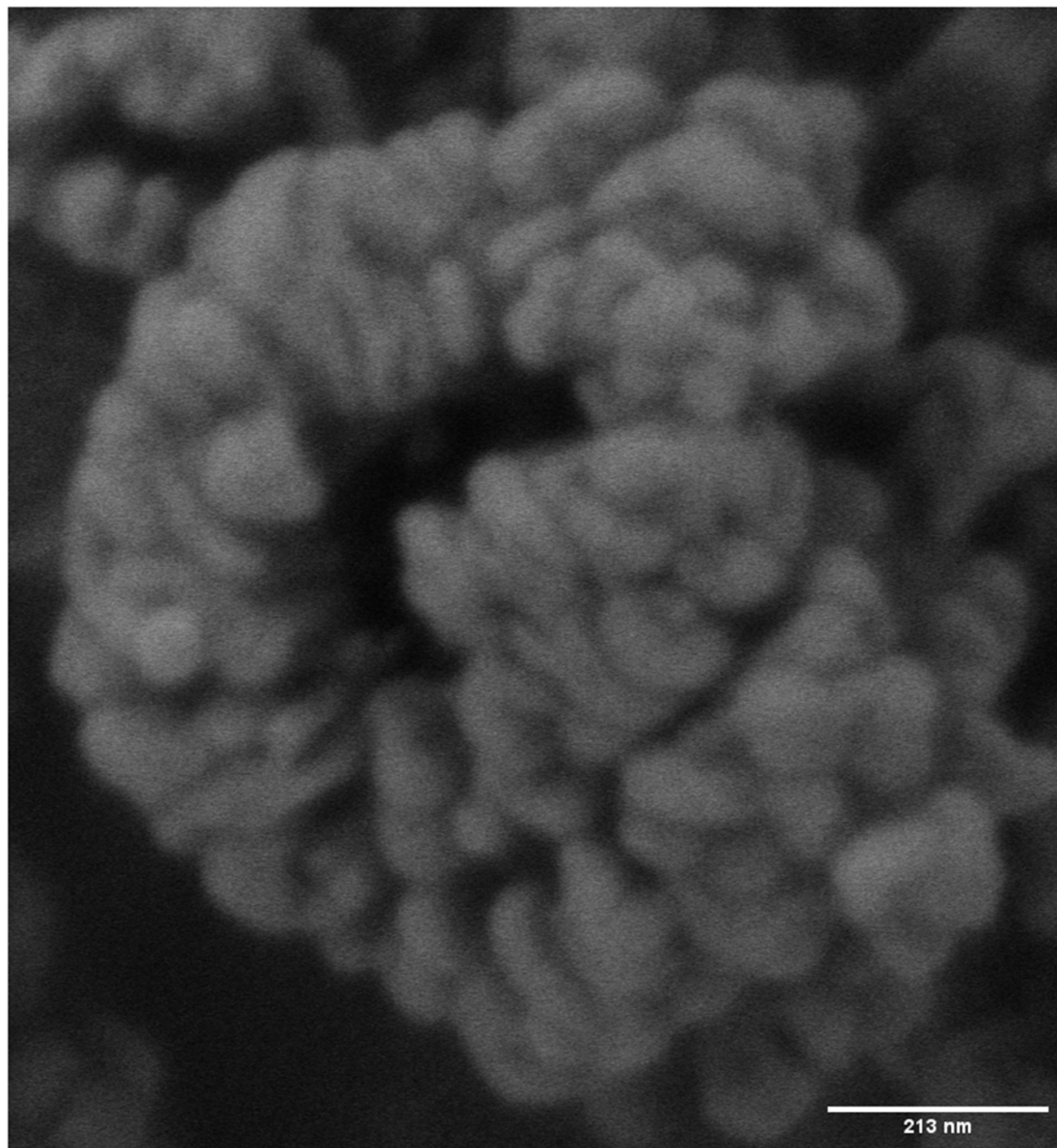
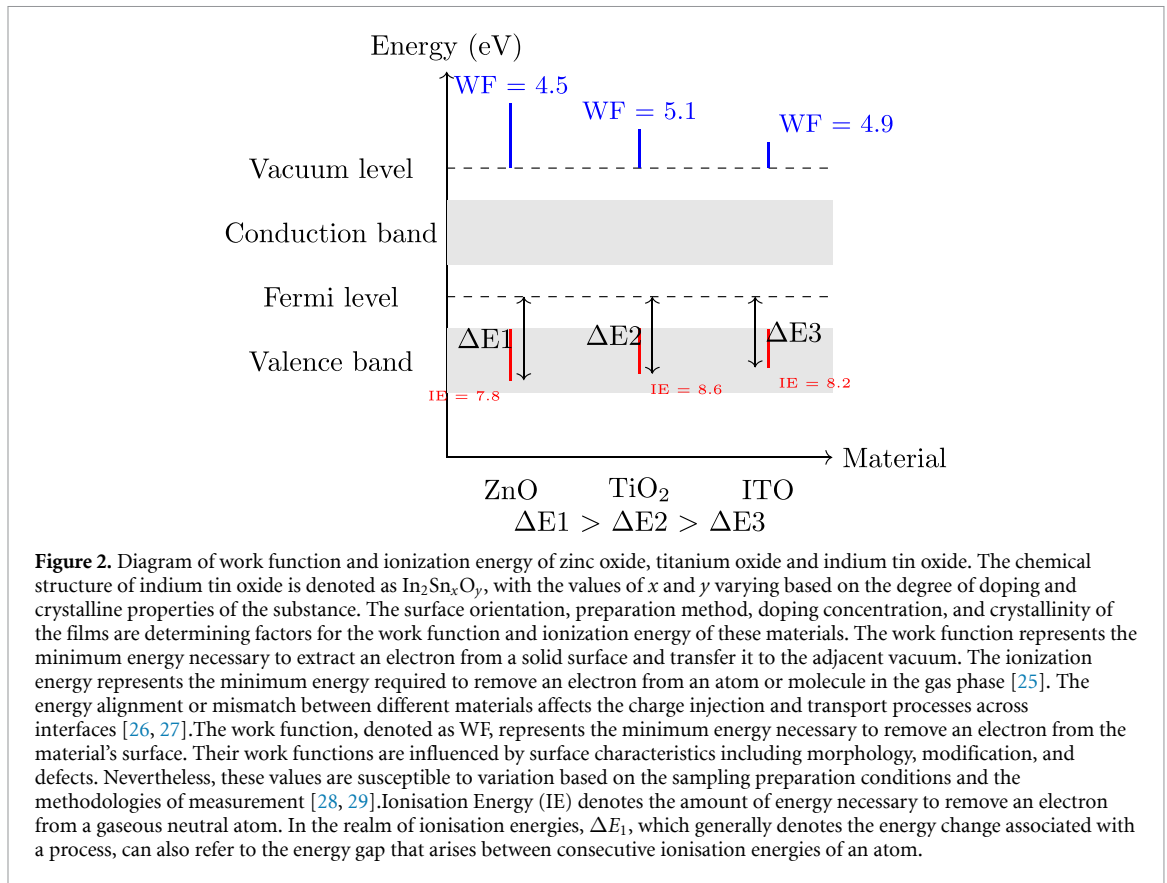


Figure 1. The SEM image depicts a cluster of proteinoids. The image depicts the intricate morphology and texture of the proteinoids' ensemble, comprising spherical units interconnected by slender filaments. The scale bar is 213 nm. The morphology of the proteinoids were analysed by scanning electron microscopy (SEM) using FEI Quanta 650 equipment. The proteinoids were characterised using Fourier transform infrared spectroscopy [9].

materials as a foundation for innovative computing systems, it is crucial to investigate their electrical spiking characteristics.

Proteinoid-ZnO interaction can alter hybrid electrical properties and trigger spiking behaviour in specific circumstances. In order to gain insight into the fundamental mechanisms of this phenomenon, it is necessary to take into account the electronic structure of commonly used materials. The diagram presented in figure 2 displays the work function and HOMO (highest occupied molecular orbital) level of the materials under investigation. These parameters are crucial in determining the charge transfer and injection at the interfaces. The aforementioned concepts will be utilised to elucidate the outcomes of our experiment and put forth a theoretical framework for the spiking mechanism of proteinoids-ZnO colloid hybrids.

Unconventional and analogue computing have gained popularity in recent years, expanding the limits of contemporary computing. This study aims to investigate whether the electro-chemical properties of proteinoid-ZnO nanocomposites facilitate electrical spiking capabilities. Our hypothesis is that the distinctive attributes of proteinoid-ZnO hybrids, namely their elevated solubility and chemical reactivity, offer a foundation for facilitating electrical spiking properties. The hypothesis is tested by combining organic materials with proteins and ZnO nanomaterials to produce electrical spiking.



2. Methods

The amino acids L-Aspartic acid and L-Glutamic acid, with 98% purity were acquired from Sigma Aldrich. Methods described in [9] were used to synthesise proteinoids.

Proteinoids (L-Glu:L-Arg) are prepared by subjecting amino acids to thermal polymerization in a dry heating environment. Usually, a blend of amino acids is mixed together in a reaction flask and subjected to temperatures ranging from 160 °C–180 °C. This triggers condensation between the amino and carboxyl groups of the amino acids, resulting in the formation of polypeptide chains. Following the heating process, the reaction mixture is subsequently cooled to room temperature prior to its dissolution in water at a temperature of 80 °C. The proteinoids undergo precipitation in the aqueous solution, which is subsequently separated using lyophilization. The proteinoid precipitate is subjected to washing procedures to eliminate contaminants, and subsequently undergoes a drying process. The final desiccated residue comprises the produced proteinoids, which can be examined using methodologies such as Fourier–transform infrared spectroscopy (FT-IR) and scanning electron microscopy (SEM). This enables the characterization of the chemical structure, composition, and morphology of the proteinoids that are generated [9].

Zinc Oxide (ZnO) nanoparticles were obtained from US Research Nanomaterials. sodium dodecyl sulphate (SDS) and sodium hydroxide (NaOH) were purchased from Merck. DMSO Pharmaceutical Grade 99.9% was obtained from Fisher Scientific. In the laboratory, de-ionized water (DIW) was generated using a Millipore unit, specifically the essential model, which provides DIW with a resistance of 15 Mohm cm. SDS was added to DIW and stirred to create a homogenous surfactant solution, resulting in a concentration of 0.22 wt% of SDS. Under continuous stirring, 2 ml of the SDS solution and 1 ml of NaOH (10 M) were added to the DMSO. While the mixture was stirred, 1 mg of ZnO nanoparticles was introduced. The resulting suspension had a constant concentration of 0.11 mg ml⁻¹. Subsequently, the suspension was placed in an ultrasonic bath for a duration of 30 min. After this step, the stirring operation was resumed and continued for several additional hours to achieve a homogeneous dispersion of ZnO particles [17, 18].

The electrical activity of the proteinoids was measured using a high-resolution data logger equipped with a 24-bit A/D converter (ADC-24, Pico Technology, UK) and iridium-coated stainless steel sub-dermal needle electrodes (Spes Medica S.r.l., Italy). Approximately 10 mm of space was left between each pair of electrodes for the purpose of measuring the electrical potential difference. One sample per second was taken to record

all electrical activity. The data recorder took an average of several readings (up to 600 per second) for further analysis.

The electrical spikes were produced using a BK 4060B function generator (B&K Precision Corporation). It's a two-channel function/arbitrary waveform generator with a host of useful features and capabilities, including the ability to produce precise sine, square, triangle, pulse, and arbitrary waveforms. It has 8 MB of memory and 16-bit resolution, making it capable of storing any waveforms. In direct digital synthesis mode, it can generate 300 MSa/s of waves, and in actual point-by-point arbitrary mode, it can generate 75 MSa/s.

Statistical analysis was implemented with ANOVA algorithm, where the terms Source, SS, DoF, MS, and F are as follows. The term Source refers to the factor that causes variation in the data. Three sources exist: Factor, Error, and Total. Factor represents the group effect (PZnO vs P). Error refers to the unexplained variation within a group caused by the factor. Total refers to the complete range of variability present within a given dataset.

SS represents the sum of squares, a metric that quantifies the degree of variability for each origin. The SS(Factor) represents the variance between the group means and the grand mean. The SS(Error) represents the total sum of squares within each group. SS(Total) represents the total variation of the data points from the grand mean, calculated as the sum of squares. The acronym DoF represents degrees of freedom, which denotes the number of independent values utilised for computing each sum of squares. The degrees of freedom for 'Factor' is calculated as the number of groups minus one, which in this case is one ($2 - 1 = 1$). The value of DoF(Error) can be calculated as the difference between the total number of observations and the number of groups, which in this case is 184 ($186 - 2 = 184$). The degrees of freedom for 'Total' is calculated as the total number of observations minus one, resulting in 185 for this particular dataset.

MS represents the mean square and is calculated by dividing each sum of squares by its corresponding degrees of freedom. The F-statistic is calculated by dividing MS(Factor) by MS(Error), where F represents the F-statistic. The F-value, calculated as the ratio of the mean square factor to the mean square error, is 17.38. The F-statistic quantifies the ratio of inter-group variance to intra-group variance. A high F-statistic suggests a significant inter-group variance.

To assess the statistical significance of the group difference, we must compare the F-statistic to a critical value derived from an F-distribution with degrees of freedom equivalent to DoF(Factor) and DoF(Error). A P-value can be utilised as an alternative, representing the likelihood of obtaining an F-statistic equal to or greater than the observed value by chance in the absence of any group differences.

3. Results

3.1. Endogenous spiking activity of proteinoids and proteinoids with colloidal zinc oxide nanoparticles

This subsection explores the inherent electrical activity of proteinoids (P) both independently and in conjunction with colloidal zinc oxide nanoparticles (ZnO). Iridium-coated stainless steel sub-dermal needle electrodes are utilised to measure exogenous potentials of P and PZnO samples without any external stimulation. We conduct an analysis of signal spiking patterns, frequency, amplitude, and synchronisation. We investigate the impact of ZnO concentration and size on the spiking behaviour of PZnO specimens. Both P and PZnO display endogenous spiking activity that resembles neuronal firing (figure 3(a)). Figure 3(b) shows the cross correlation versus time lags for the electrical activity of proteinoids alone compared to the proteinoid-ZnO (PZnO) mixture. The cross correlation provides information on the similarity of the signals as a function of shifting one signal in time relative to the other. The addition of ZnO increases the spiking frequency and synchronisation of P, as will be evidenced further, indicating that ZnO may act as a modulator of P's electrical properties.

Table 1 displays the outcomes of a one-way ANOVA, which compares the means of two groups, namely 1:PZnO and 2:P. ANOVA assesses group differences. The ANOVA's P-value is 0.000, indicating a low probability of observing a significant F-statistic under the assumption of no difference between PZnO and P. The null hypothesis of no difference between PZnO and P can be rejected, indicating a significant difference.

The electrical activity of the proteinoid-ZnO (PZnO) mixture and proteinoid (P) alone are compared in figure 4. The box plots illustrate the distribution of voltage responses for each sample, with the first box showing PZnO and the second showing P. As seen in the figure, PZnO exhibits a higher median voltage (0.24 mV) compared to P (0.13 mV). Additionally, the voltage response of PZnO has a wider distribution, with the first quartile at 0.11 mV, second quartile at 0.24 mV, and third quartile at 0.42 mV. In contrast, the quartiles for P are tighter, ranging from 0.07 mV (first quartile) to 0.21 mV (third quartile). This indicates the PZnO mixture displays greater electrical activity overall than the proteinoid alone, with a broader range of voltage responses. The outliers in the box plots further highlight the wider distribution and more variable voltage activity of the PZnO composite.

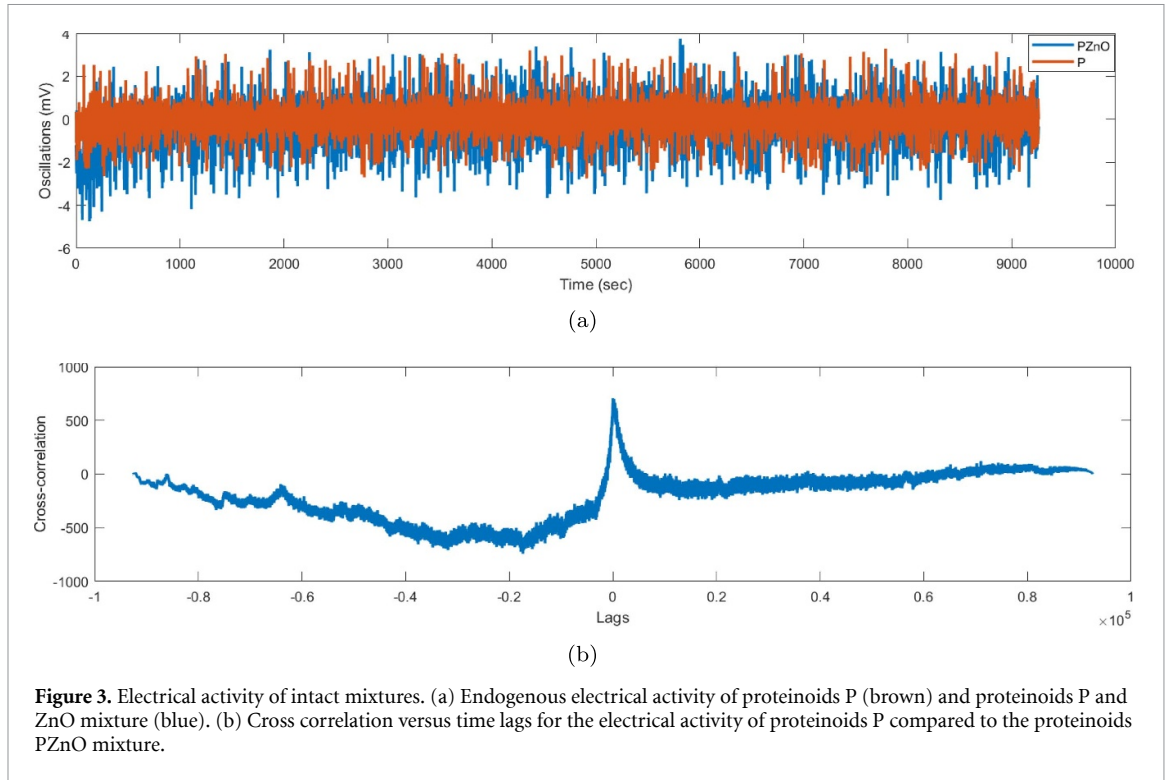
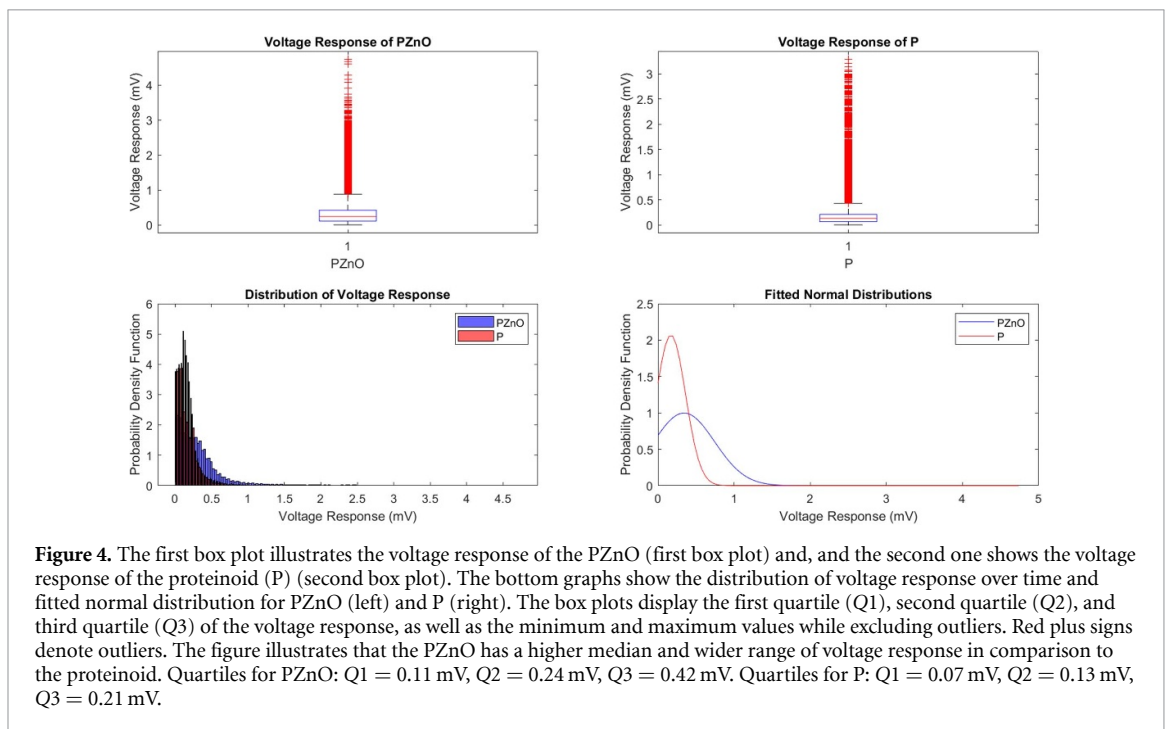


Table 1. The results of a one-way ANOVA comparing the means of two groups, namely 1:PZnO and 2:P, are presented. The statistical analysis reveals a significant difference between the groups at a significance level of 0.05, as indicated by the F-statistic and P-value.

Source	SS	DoF	MS
Factor	2.5822+03	1	2.5822+03
Error	2.7361+04	185 202	0.1477
Total	2.9943+04	185 203	—

SS: sum of squares; DoF: degrees of freedom; MS: mean square.



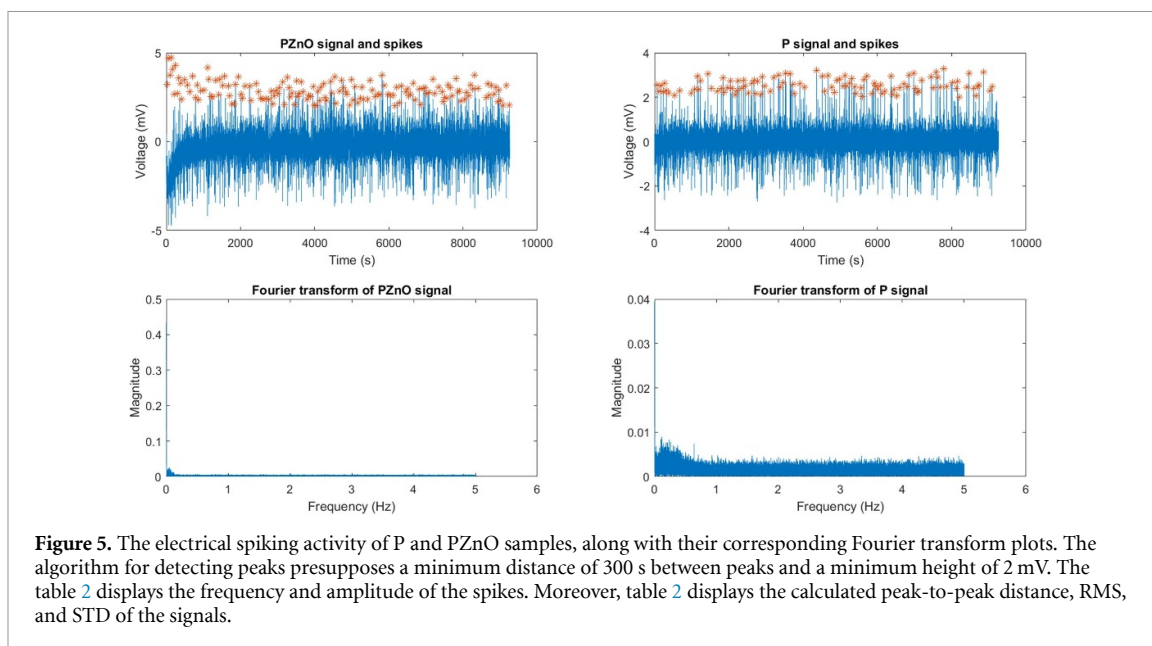


Figure 5. The electrical spiking activity of P and PZnO samples, along with their corresponding Fourier transform plots. The algorithm for detecting peaks presupposes a minimum distance of 300 s between peaks and a minimum height of 2 mV. The table 2 displays the frequency and amplitude of the spikes. Moreover, table 2 displays the calculated peak-to-peak distance, RMS, and STD of the signals.

Table 2. Comparison of frequency, amplitude, peak to peak distance, RMS, and STD of PZnO, P and ZnO signals.

Signal	Frequency (mHz)	Amplitude (mV)	Peak to peak (mV)	RMS (mV)	STD (mV)
PZnO	19.1	2.8611	8.4916	0.5262	0.4796
P	15.6	2.5399	6.0335	0.2565	0.2558
ZnO	2.05	11.38	10.31	11.52	1.81

PZnO exhibits a greater endogenous spiking response than P, as indicated by the quartiles in figure 4. The median of PZnO is 0.24 mV, exceeding the third quartile of P at 0.21 mV. This implies that the voltage response of 75% or more of PZnO is greater than that of 75% or more of P. PZnO exhibits a broader voltage response range compared to P. The interquartile range of PZnO (0.31 mV) is greater than that of P (0.14 mV). PZnO exhibits greater voltage response variability compared to P.

PZnO shows a more robust oscillatory response to endogenous spiking than P, as evidenced by its slightly higher frequency and amplitude of spikes in figure 5 and table 2. The PZnO signal exhibits a greater dynamic range and variability in voltage fluctuations compared to the P signal, as evidenced by its higher peak-to-peak distance, RMS, and STD. The results suggest that PZnO exhibits greater sensitivity and responsiveness to endogenous spiking than P, and possesses a more intricate temporal coding of information.

The SPIKY Matlab program [30, 31] was employed to assess the spike train synchrony of proteinoid and ZnO nanoparticles colloid (PZnO)/proteinoid (P) samples. Two metrics, SPIKE synchronisation and ISI-distance, were utilised to quantify synchrony. SPIKE synchronisation and ISI-distance are measures of spike train synchrony and dissimilarity, respectively. SPIKE synchronisation ranges from 0 to 1, with 0 indicating no synchrony and 1 indicating perfect synchrony. ISI-distance ranges from 0 to 1, with 0 indicating identical spike trains and 1 indicating no similarity between spike trains [32].

Figure 6 displays the SPIKE synchronisation values over time for the spike trains of PZnO and P samples. The mean SPIKE synchronisation throughout the recording period is 0.2791, indicating a moderate level of synchrony between the spike trains. The plot displays the peaks and spike timing for each sample, distinguishing between PZnO and P samples.

The ISI-distance values for each pair of spikes from spike trains PZnO and P, computed by the SPIKY Matlab program, are presented in figure 7. The mean ISI-distance throughout the recording period is 0.4324, indicating a moderate level of dissimilarity among the spike trains.

The SPIKY program was utilised to assess the synchronicity of spike trains in Proteinoids-ZnO colloidal nanoparticles across varying conditions. Figure 8 demonstrates that zinc oxide addition resulted in lower SPIKE-distance values compared to proteinoids, indicating greater similarity in spike trains. ZnO addition increases the electrical spiking activity of Proteinoids-ZnO colloidal nanoparticles. The sorted pairwise matrix D indicates that the samples treated with ZnO formed a distinct cluster from the other samples, providing additional evidence to support this observation. The findings align with prior research indicating non-trivial activity of ZnO nanocrystals [33–35].

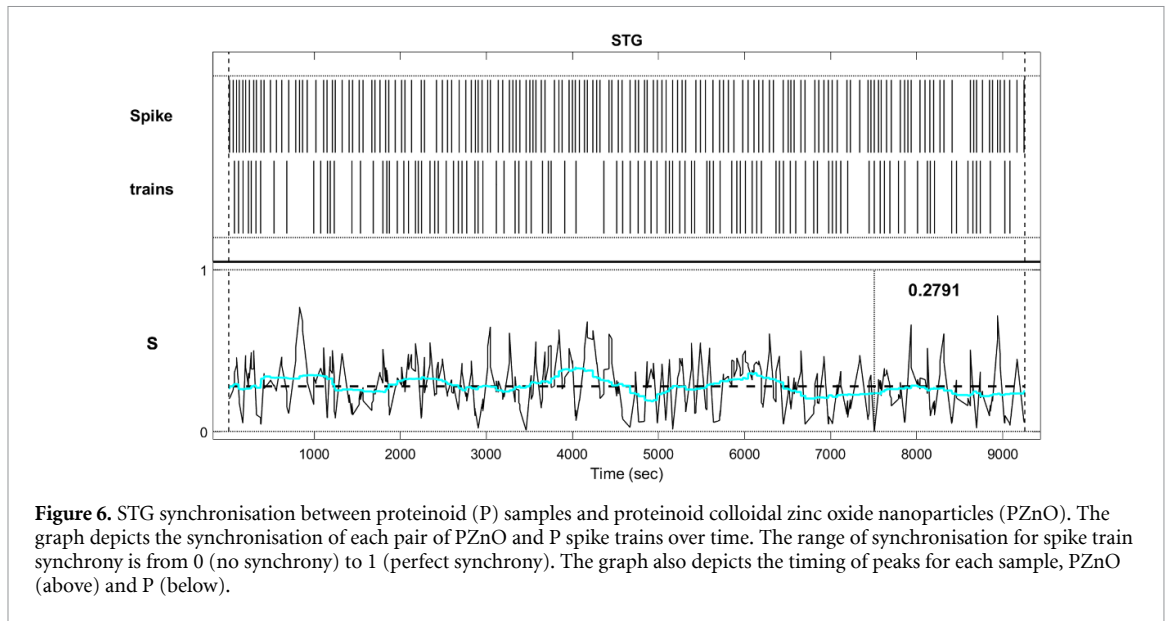


Figure 6. STG synchronisation between proteinoid (P) samples and proteinoid colloidal zinc oxide nanoparticles (PZnO). The graph depicts the synchronisation of each pair of PZnO and P spike trains over time. The range of synchronisation for spike train synchrony is from 0 (no synchrony) to 1 (perfect synchrony). The graph also depicts the timing of peaks for each sample, PZnO (above) and P (below).

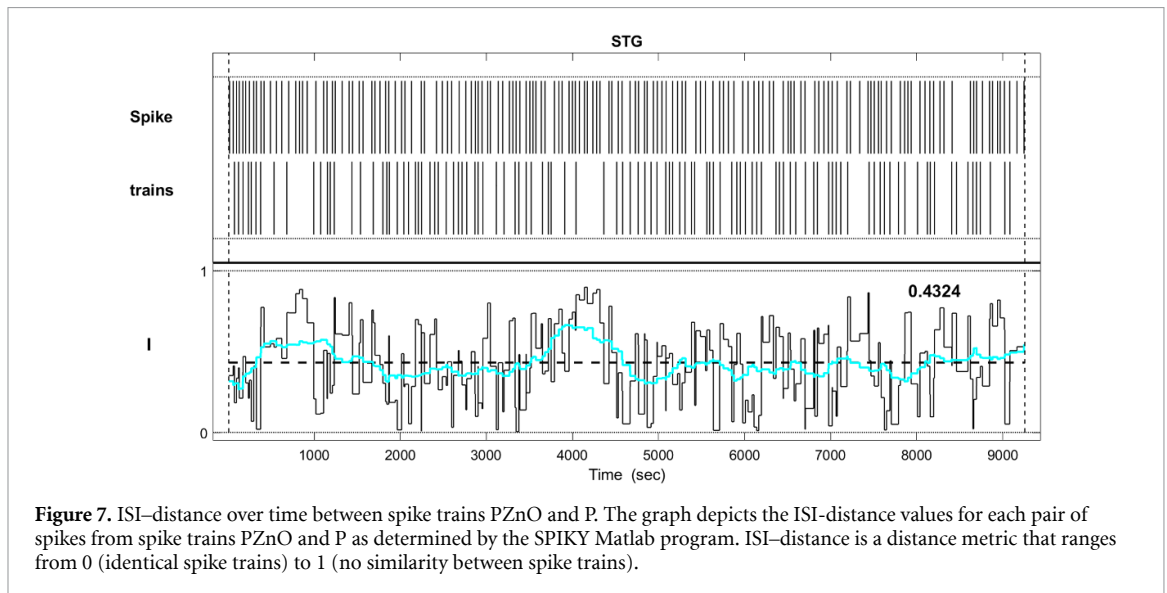


Figure 7. ISI-distance over time between spike trains PZnO and P. The graph depicts the ISI-distance values for each pair of spikes from spike trains PZnO and P as determined by the SPIKY Matlab program. ISI-distance is a distance metric that ranges from 0 (identical spike trains) to 1 (no similarity between spike trains).

SPIKY produces spike trains by identifying peaks in the signals that surpass a predetermined threshold (figure 6). The programme proceeds to compute various metrics for comparing spike trains, such as the instantaneous SPIKE-distance profile (figure 6), the pairwise distance matrix D (figure 8), and the sorted distance matrix obtained by optimising \cdot . SPIKY utilises hierarchical clustering on the sorted SPIKE-distance matrix to split the spike trains into clusters that exhibit various spiking characteristics (figure 7). Ultimately, statistical analysis is used to identify the groupings that display noteworthy disparities in spiking patterns (figure 8). Our data demonstrate distinct separation between the spike trains of PZnO and proteinoids (P), as revealed by SPIKY. The PZnO action is clearly separate from the proteinoids, and this distinction is statistically significant ($p < 0.05$). The results illustrate the usefulness of SPIKY in measuring variations in intricate electrical activity resulting from diverse nano-bio interactions. The technique's capacity to differentiate between PZnO and proteinoids affirms its ability to distinguish unique mechanisms of interfacial electron transport in these hybrid systems.

The findings indicate a moderate resemblance between the spike trains of PZnO and P samples, but insufficient evidence to suggest significant synchronisation. The observed variation could be attributed to the distinct characteristics of proteinoid colloidal zinc oxide nanoparticles and proteinoid samples, including their size, shape, charge, or STG (Spike Train Generator) neuron interaction. Additional research is required to investigate the mechanisms and impacts of these nanoparticles on STG activity and function.

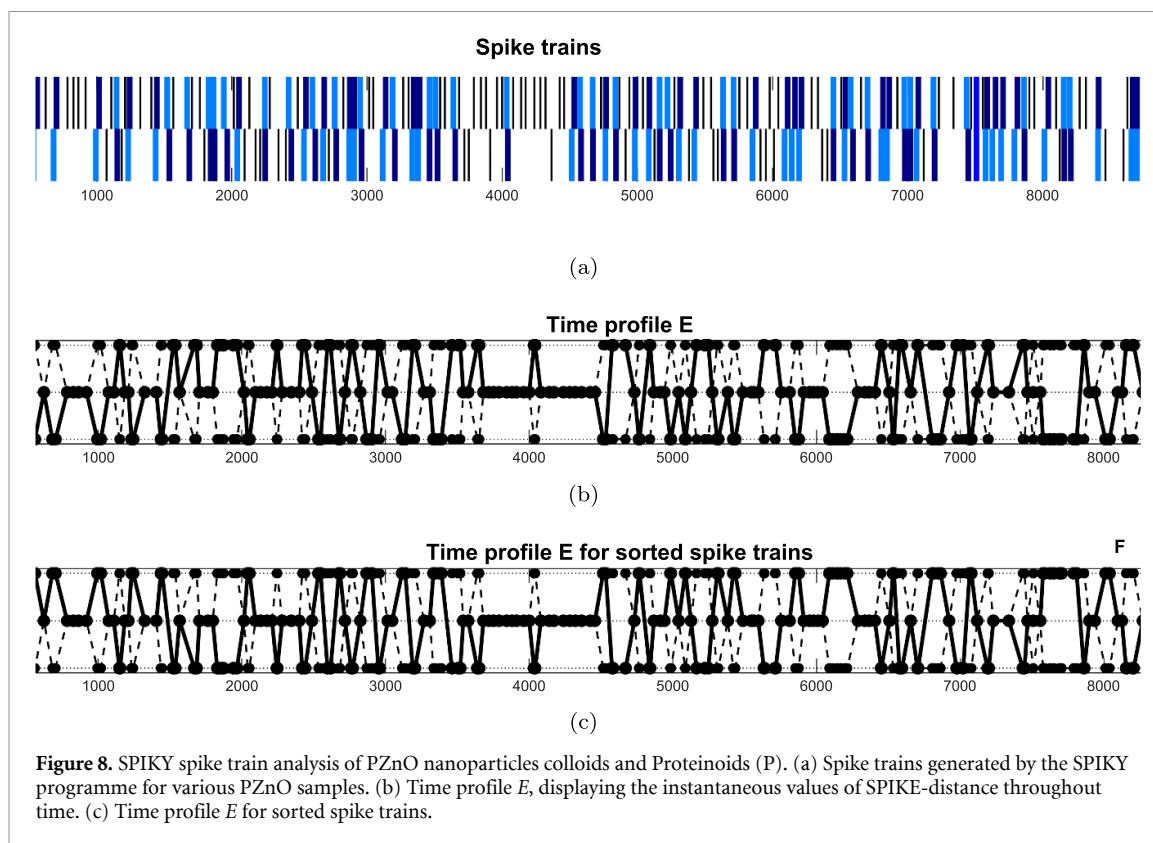


Figure 8. SPIKY spike train analysis of PZnO nanoparticles colloids and Proteinoids (P). (a) Spike trains generated by the SPIKY programme for various PZnO samples. (b) Time profile E , displaying the instantaneous values of SPIKE-distance throughout time. (c) Time profile E for sorted spike trains.

3.2. Response to electrical stimulation of proteinoids and proteinoids with colloidal zinc oxide nanoparticles

This subsection investigates the reaction of proteinoids (P) and proteinoids containing colloidal zinc oxide nanoparticles (ZnO) to external electrical stimulation. A voltage pulse generator is utilised to administer varied intensities and frequencies of stimuli to P and PZnO samples on microelectrode arrays. We assessed alterations in spiking activity, latency, and threshold of P and PZnO pre-, during, and post-stimulation. We assessed the response of P and PZnO compared to biological neurons and analysed the impact of ZnO concentration and size on the response of PZnO spikes. Both P and PZnO exhibit dose-dependent and frequency-dependent responses to electrical stimulation. The findings suggest that ZnO amplifies the excitability of P, as evidenced by the lower threshold and higher sensitivity to stimulation of PZnO compared to P.

Figure 9 illustrates the dissimilar oscillation patterns and low correlation between the proteinoid (first plot) and device input (second plot). This implies a lack of synchronisation or mutual influence between the hybrid and the proteinoid. This result aligns with prior research indicating that proteinoids are self-organising entities with intricate dynamics [36, 37]. This finding contradicts hypotheses suggesting that proteinoids can respond to external stimuli and adjust their oscillations accordingly. One plausible reason for this inconsistency is the inadequacy or insensitivity of the hybrid employed in the study to trigger modifications in the proteinoid's response. This study's strength lies in the utilisation of a novel cross-correlation method to assess the association between the PZnO and proteinoid, a previously unexplored approach. This study is limited by its use of a single hybrid and proteinoid type, potentially restricting the applicability domain of the findings. Subsequent studies may investigate various hybrids and proteinoids, along with diverse parameters and conditions, to examine the potential interactions and applications of these systems.

Table 3 indicates a significant disparity between the average voltage of the proteinoid and the hybrid. The obtained p -value (2.0768×10^{-21}) is below the predetermined significance level of 0.05, indicating that the null hypothesis of equal mean voltage between the proteinoid and the hybrid can be rejected. The rejection is confirmed by the test result $h = 1$. The proteinoid has a mean voltage of -0.5516 mV, whereas the hybrid has a mean voltage of -7.6795 mV, indicating a significant voltage difference between the two (figure 10). The dissimilarity may arise from the distinct characteristics and operations of the proteinoid and the hybrid, including their arrangement, conductance, and reaction to environmental signals. Additional investigation

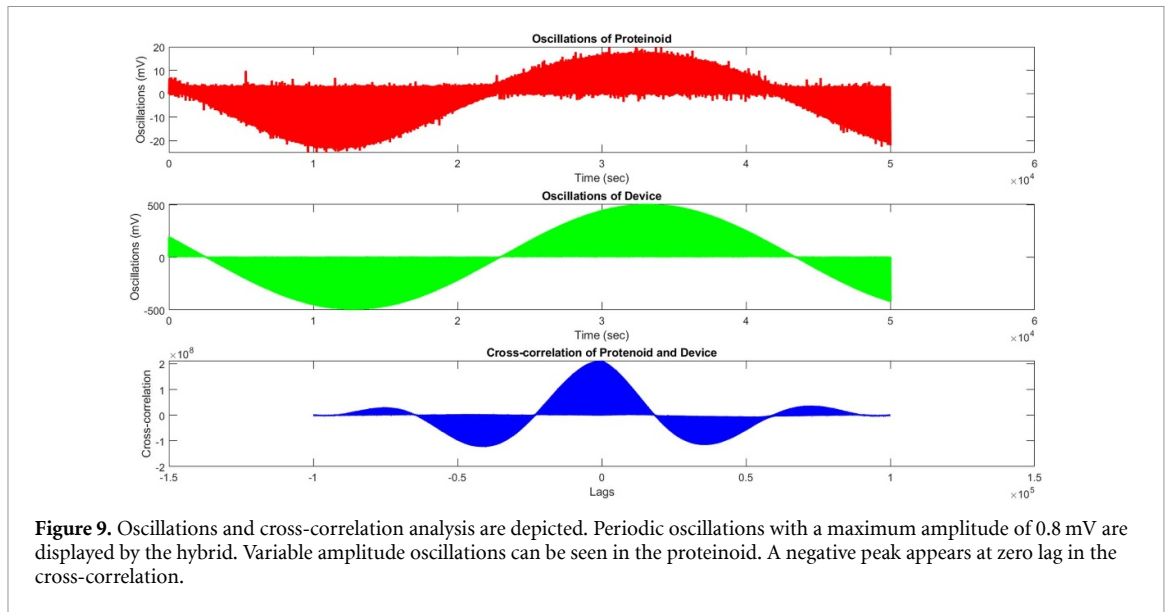
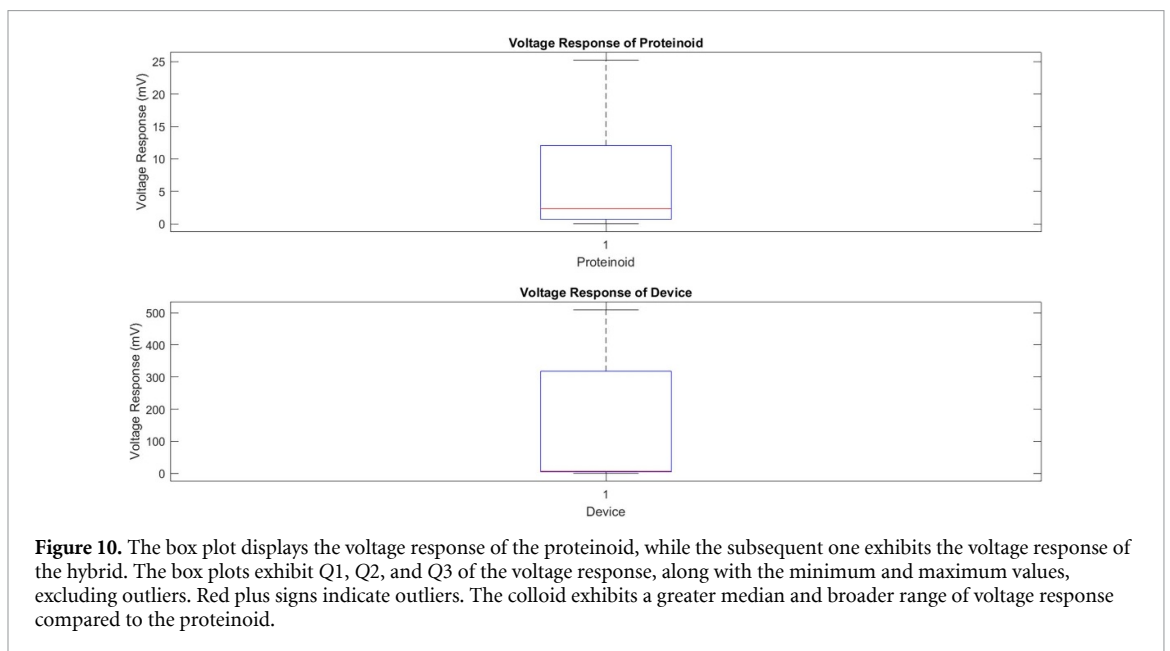


Table 3. A summary of variance analysis.

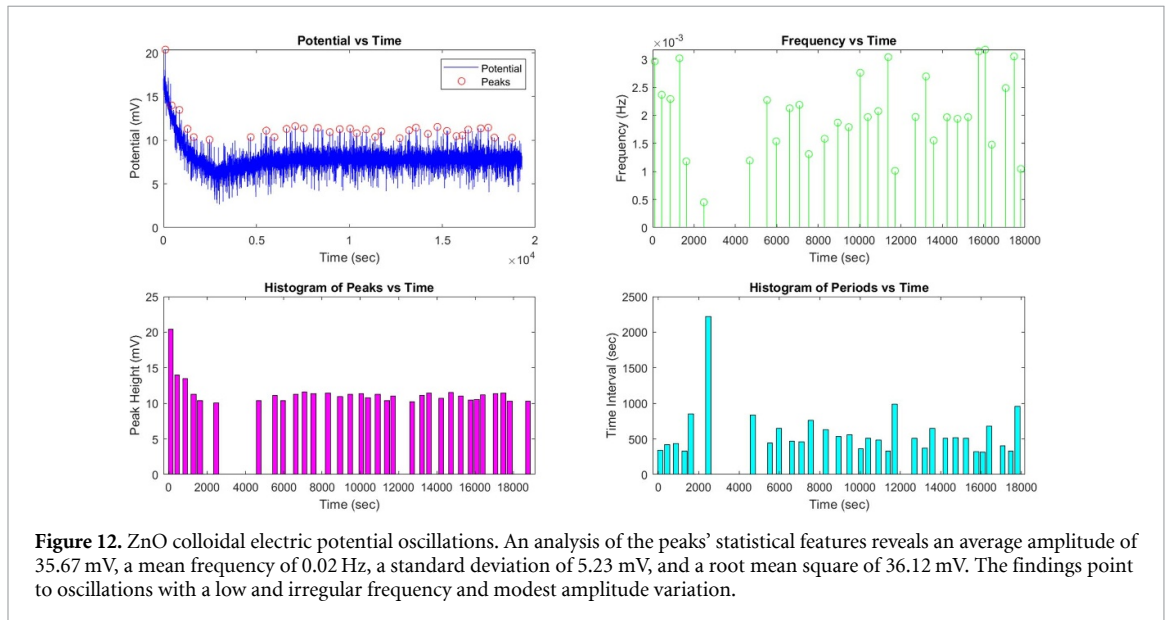
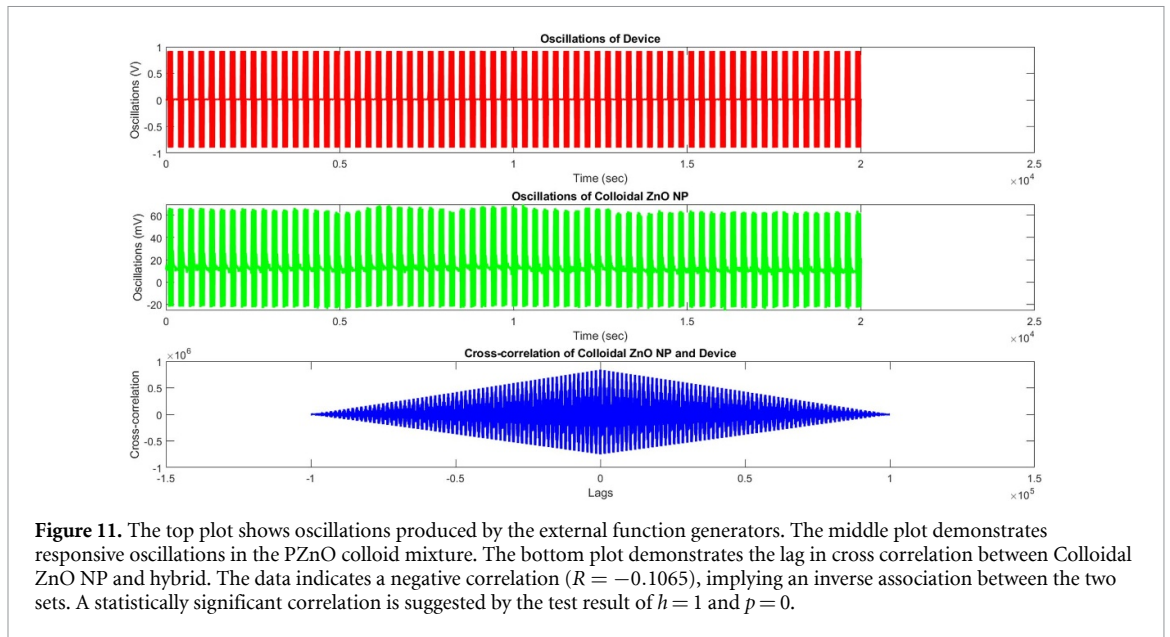
Source	SS	df	MS
Columns	$2.5406 \times 10^{+06}$	1	$2.5406 \times 10^{+06}$
Error	$5.6277 \times 10^{+09}$	200 010	$2.8137 \times 10^{+04}$
Total	$5.6303 \times 10^{+09}$	200 011	—

SS: sum of squares; df: degrees of freedom; MS: mean square.



may examine the determinants impacting the voltage of both systems and their potential modulation or regulation for practical purposes.

Figure 11 depicts the reaction of the PZnO colloid mixture to oscillatory signals applied by function generators. The first plot displays the reference oscillations, whereas the second plot illustrates the measured oscillations in the colloidal mixture. The cross-correlation analysis in the lower figure indicates a negative correlation ($R = -0.1065$) between the input and output signals, suggesting an inverse link. The statistical test verifies a substantial association with a coefficient of $h = 1$ and a p -value of 0. Figure 12 displays the inherent electrical oscillations that were recorded in the ZnO nanoparticle colloids. The oscillation peaks



were analysed to provide the following statistics: an average amplitude of 35.67 millivolts (mV), a mean frequency of 0.02 Hertz (Hz), a standard deviation of 5.23 mV, and a root mean square of 36.12 mV. These measurements indicate that the colloidal oscillations exhibit frequencies that are quite low and irregular, with modest fluctuations in amplitude.

The oscillations of proteinoid (L-Glu:L-Arg) and stimulating device were measured in response to a square wave function. Figure 13 displays the time series and cross-correlation of the oscillations. The mean voltage of proteinoid oscillations was 0.52 mV, whereas that of hybrid oscillations was 9 mV. The cross-correlation analysis indicated a significant negative correlation between the two signals, with a correlation coefficient of -0.2583 and a p -value of 1.2526×10^{-10} (table 4).

An ANOVA was conducted to examine the correlation between proteinoid and hybrid oscillations. Table 5 presents the ANOVA results. The variance of the columns source was $3.6043 \times 10^{+06}$ units, significantly higher than the error variance of $8.7091 \times 10^{+04}$ units. The F-statistic of 41.3855 indicates significant difference between the proteinoid and hybrid oscillations.

The findings indicate an inverse correlation between proteinoid and hybrid oscillations, with proteinoid oscillations exhibiting greater sensitivity to square wave function to hybrid oscillations.

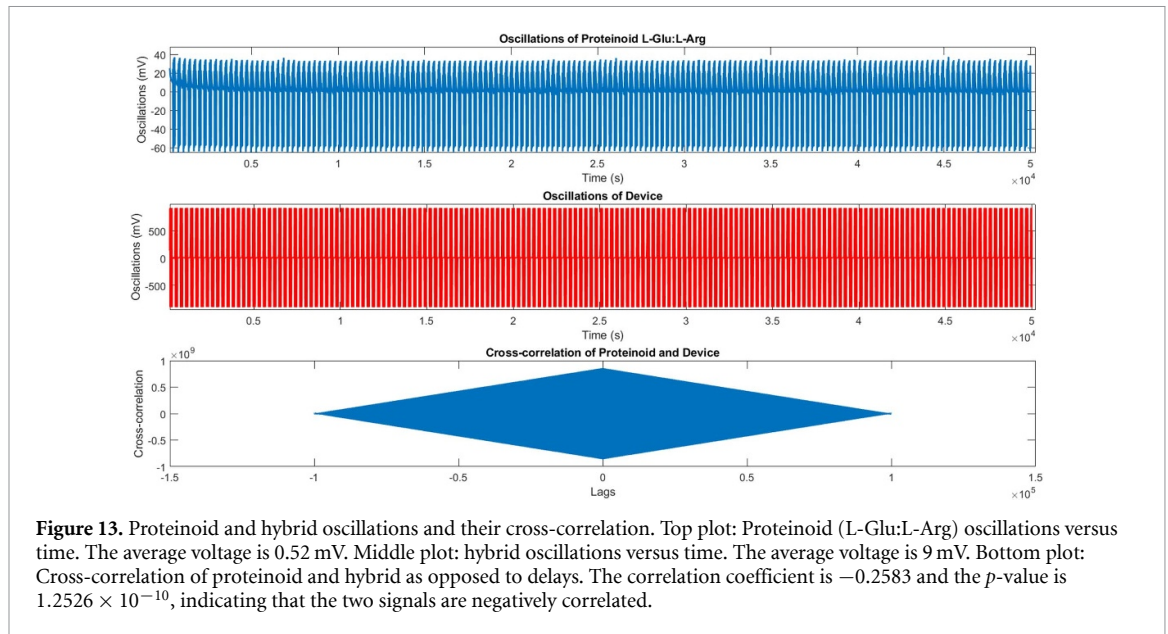


Figure 13. Proteinoid and hybrid oscillations and their cross-correlation. Top plot: Proteinoid (L-Glu:L-Arg) oscillations versus time. The average voltage is 0.52 mV. Middle plot: hybrid oscillations versus time. The average voltage is 9 mV. Bottom plot: Cross-correlation of proteinoid and hybrid as opposed to delays. The correlation coefficient is -0.2583 and the p -value is 1.2526×10^{-10} , indicating that the two signals are negatively correlated.

Table 4. ANOVA table for cross-correlation analysis of ZnO colloid oscillations and the stimulating device. The data indicates a significant negative correlation ($R = -0.1065$) between the two series, suggesting an inverse relationship.

Source	SS	df	MS	F	Prob>F
Columns	$9.3903 \times 10^{+06}$	1	$9.3903 \times 10^{+06}$	$4.5234 \times 10^{+04}$	0
Error	$4.1520 \times 10^{+07}$	200 010	207.5918	—	—
Total	$5.0911 \times 10^{+07}$	200 011	—	—	—

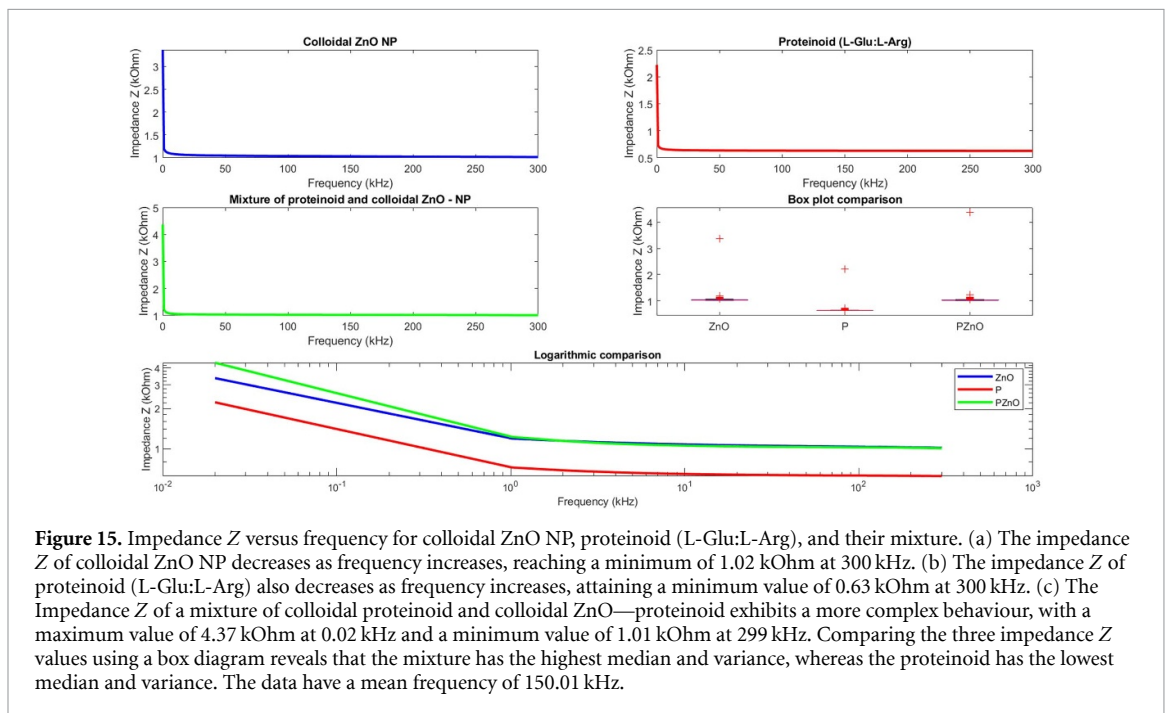
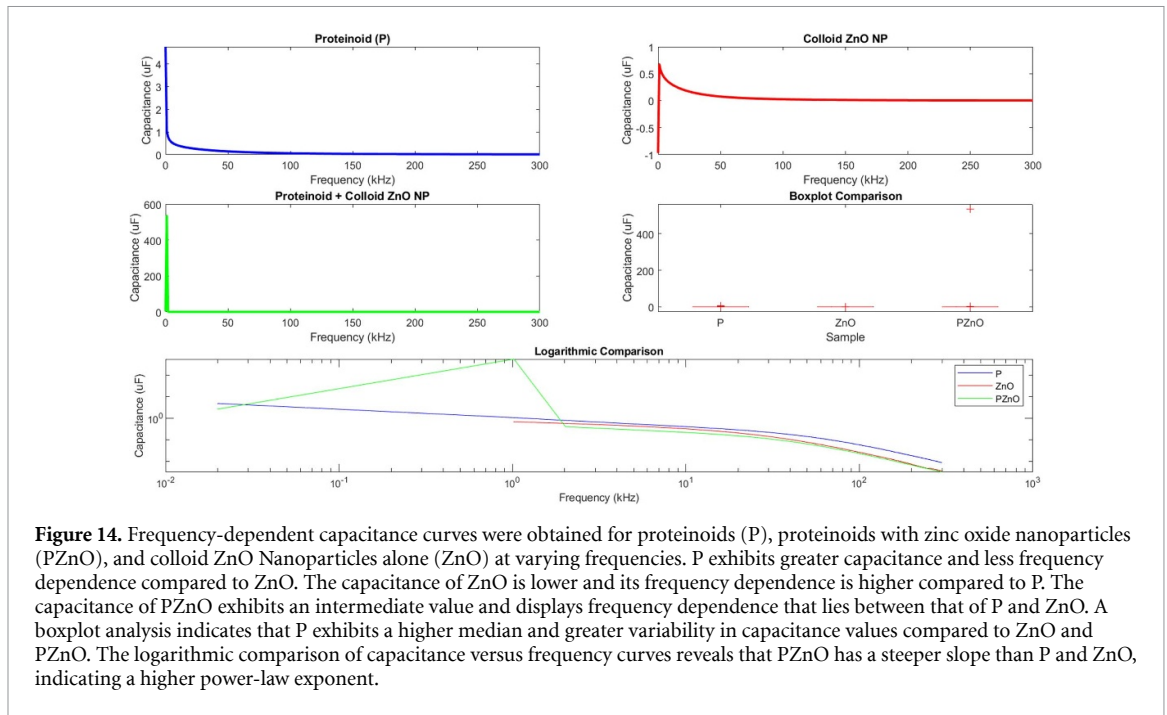
Table 5. Cross correlation of oscillation of proteinoid (L-Glu:L-Arg) and hybrid.

Source	SS	df	MS	F	Prob>F
Columns	$3.6043 \times 10^{+06}$	1	$3.6043 \times 10^{+6}$	41.3855	1.2526×10^{-10}
Error	$1.7419 \times 10^{+10}$	200 010	$8.7091 \times 10^{+04}$	—	—
Total	$1.7423 \times 10^{+10}$	200 011	—	—	—

3.3. Capacitance and impedance measurements of proteinoids, proteinoids with zinc oxide nanoparticles, and zinc oxide nanoparticles at various frequencies

The figure 14 depicts the capacitance vs frequency curves for each sample in a subplot, as well as boxplot and logarithmic comparisons. We can see from the results and the figure that: among the three samples, the PZnO hybrid (mixture of proteinoid L-Arg:L-Glu and Zinc oxide colloidal nanoparticles) sample has the highest max capacitance value ($535 \mu\text{F}$) and the lowest min capacitance value ($0.0032 \mu\text{F}$). This indicates that the capacitance values in the PZnO sample vary depending on the frequency. The P (proteinoid L-Glu:L-Arg) sample has the lowest maximum capacitance value ($4.753 \mu\text{F}$) and the highest minimum capacitance value ($0.0086 \mu\text{F}$) among the three samples. This suggests that frequency limits the capacitance values in the P sample. The colloidal ZnO nanoparticle sample (ZnO) has an intermediate maximum capacitance value ($0.6765 \mu\text{F}$) and a negative minimum capacitance value ($-0.9719 \mu\text{F}$) among the three samples. This suggests that the ZnO sample has a moderate range of capacitance values based on frequency, but at low frequencies it exhibits some peculiar behaviour known as negative capacitance, already observed by some of us [9, 38]. All samples have maximum capacitance values at low frequencies (0.02 kHz or 1.02 kHz), while all samples have minimum capacitance values at high frequencies (300 kHz). This implies that for these samples, capacitance and frequency have an inverse relationship. A boxplot comparison reveals that the P sample has a substantially higher median and interquartile range than the mixture of PZnO, indicating that it has a higher average capacitance and more variability. The logarithmic comparison reveals that the P sample has a steeper slope than the PZnO sample, indicating that it has a faster rate of change of capacitance with respect to frequency.

It is conceivable to draw the following conclusions from these data: When compared to the P and ZnO samples, the PZnO sample has higher capacitance efficiency because it can store and discharge more charge at low and high frequencies. The PZnO sample had higher capacitance values than either component alone,



suggesting that the combination of proteinoid and zinc oxide nanoparticles has a synergistic impact. The ZnO sample features oxygen vacancies that together with its ferroelectric nature enable negative capacitance at low frequencies, which is not typical for perfect capacitors [39–41].

At various frequencies between 0.02 and 300 kHz, the impedance Z of colloidal ZnO, proteinoid (L-Glu:L-Arg), and their mixture was determined. Figure 15 displays the obtained outcomes. If the electrical conductivity is high, the impedance Z will be low, and vice versa [42]. Both colloidal ZnO and proteinoid (L-Glu:L-Arg) exhibited a relevant capacitive behaviour [43], with their impedance Z decreasing with increasing frequency. Additional elements, such as interfacial polarisation or charge transfer [44], may be influencing the electrical properties of the mixture because the impedance Z of the mixture displayed a more complex pattern. The median and variability of impedance Z were both largest for the combination, while they were both lowest for the proteinoid in the box plot comparison. This suggests that the mixture is more structurally and compositionally diverse than the individual components.

Table 6. Summary of impedance measurements for colloidal ZnO NP, proteinoid (L-Glu:L-Arg), and their mixture at different frequencies.

Material	ZMean (kOhm)	ZMax (kOhm)	ZMin (kOhm)	ZStd (kOhm)
ZnO	1.04	3.36	1.02	0.67
P	0.64	2.22	0.63	0.46
PZnO	1.04	4.37	1.01	0.97

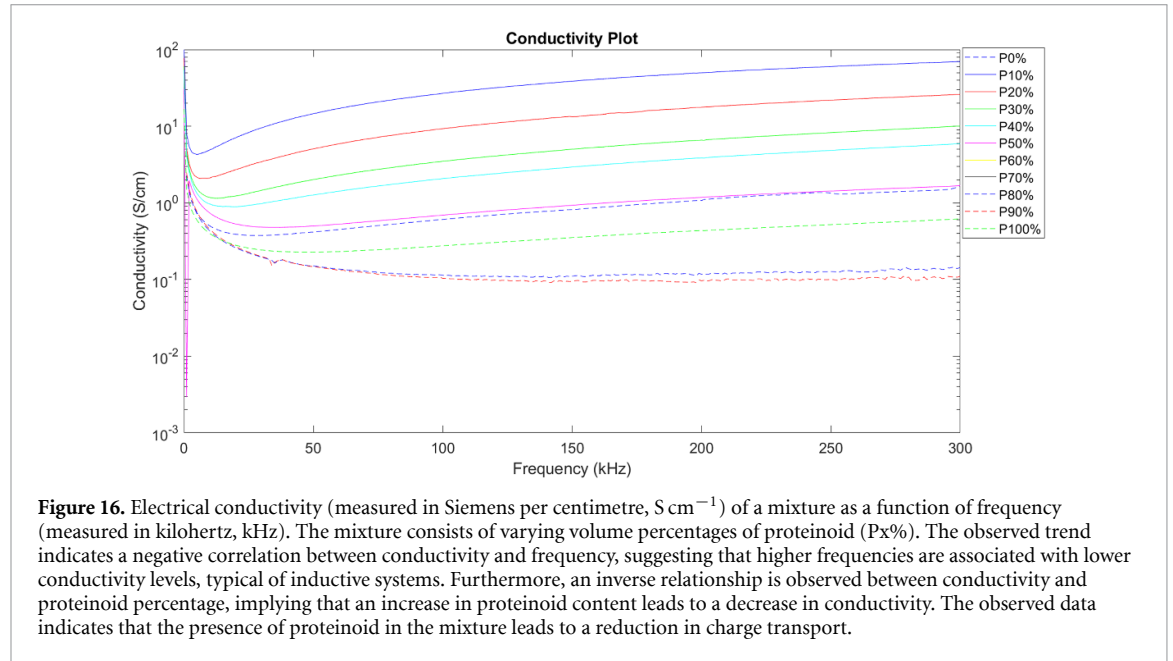
**Figure 16.** Electrical conductivity (measured in Siemens per centimetre, $S\text{ cm}^{-1}$) of a mixture as a function of frequency (measured in kilohertz, kHz). The mixture consists of varying volume percentages of proteinoid (Px%). The observed trend indicates a negative correlation between conductivity and frequency, suggesting that higher frequencies are associated with lower conductivity levels, typical of inductive systems. Furthermore, an inverse relationship is observed between conductivity and proteinoid percentage, implying that an increase in proteinoid content leads to a decrease in conductivity. The observed data indicates that the presence of proteinoid in the mixture leads to a reduction in charge transport.

Table 6 summarises the average, maximum, and minimum impedance Z values, as well as the frequencies at which they occur, for each material. In addition, we present the standard deviation of the mean Z values for the impedance. Data averaged out to 150.01 kHz in terms of frequency. Colloidal ZnO NP, proteinoid (L-Glu:L-Arg), and their mixture all reached their highest impedance Z values of 3.36, 2.22, and 4.37 kOhm at 0.02 kHz. The lowest values of impedance Z were recorded at 300, 300, and 299 kHz for colloidal ZnO NP, proteinoid (L-Glu:L-Arg), and their mixture, respectively.

Both the no-electrical-stimulation control condition and the electrically-stimulated experimental condition cannot be explained mechanistically by the data alone. However, here are some hypotheses to consider: In the absence of electrical stimulation, the impedance Z rises and the electrical conductivity falls because the proteinoids and colloidal particles interact less. By increasing the contact between the colloidal particles and the proteinoid molecules, an electrical field can increase the channels through which charges can flow and decrease the impedance Z . Stimulating materials electrically can cause structural changes like dipole alignment or aggregate development, which can alter their electrical properties in various ways. These hypotheses need to be tested experimentally, and the mechanism of electrical stimulation of these materials needs to be clarified. Further we demonstrate our approach to test the hypothesis.

The conductivity of the samples was estimated from the capacitance measurements using the following formula:

$$\sigma = \frac{1}{\omega C \sqrt{1 + \tan^2(\phi)}}$$

where σ is the conductivity in $S\text{ cm}^{-1}$, ω is the angular frequency in rad s^{-1} , C is the capacitance in F, and ϕ is the phase angle in radians. The frequency range was from 0 to 300 kHz [45, 46].

The present study aimed to investigate the frequency-dependent conductivity of a mixture comprising proteinoid-zinc oxide colloidal nanoparticles. The experimental setup involved varying the volume percentages of proteinoid (Px%) in order to assess its influence on the conductivity measurements. The findings are visually represented in figure, 16. The observed data in the figure indicates a negative correlation between conductivity and frequency, as well as conductivity and proteinoid percentage. The highest observed conductivity was recorded for the sample with P0% composition at a frequency of 0.2 kHz, yielding a conductivity value of 77.4 S cm^{-1} . The experimental results indicate that the highest resistivity was observed

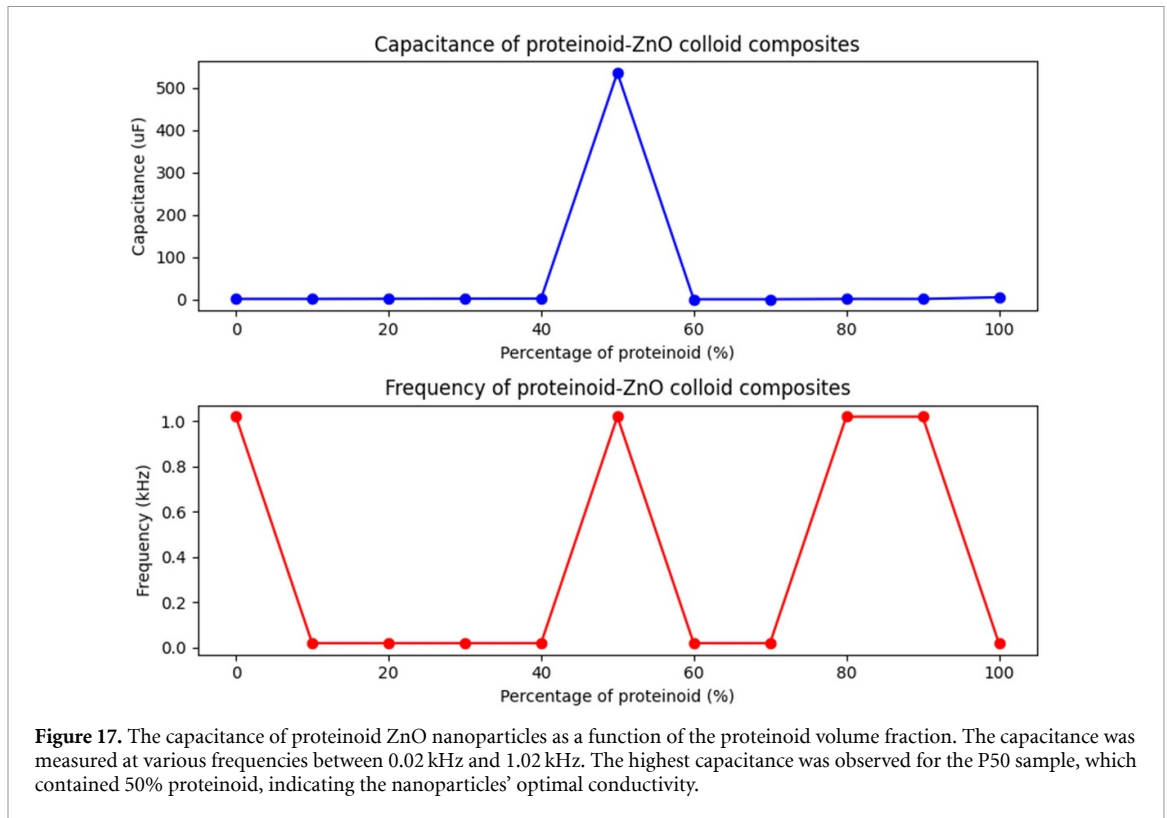


Figure 17. The capacitance of proteinoid ZnO nanoparticles as a function of the proteinoid volume fraction. The capacitance was measured at various frequencies between 0.02 kHz and 1.02 kHz. The highest capacitance was observed for the P50 sample, which contained 50% proteinoid, indicating the nanoparticles' optimal conductivity.

for the sample labelled as P90% when subjected to a frequency of 300 kHz. The obtained value for the conductivity of this sample was measured to be 0.108 S cm^{-1} .

As depicted in figure 17, it is evident that the capacitance of the nanoparticles exhibited an upward trend as the proteinoid content was augmented, reaching its peak at 50%. Subsequently, a pronounced decline in capacitance was observed for higher proteinoid content. The sample denoted as P50% exhibited the highest capacitance among the tested samples. This finding suggests that the presence of 50% proteinoid in the mixture resulted in the most favourable conductivity characteristics of the nanoparticles. The observed capacitance exhibited an apparent dependence on the frequency of the measurement, whereby an increase in frequency corresponded to a decrease in capacitance values across the majority of the samples. The findings of this study indicate that the conductivity of proteinoid zinc oxide colloidal nanoparticles can be adjusted, or 'tuned', based on two factors: the amount of proteinoid present and the frequency of the electric field being applied. The utilisation of these nanoparticles holds promise in the development of innovative biosensors and nanoelectronic devices. Nevertheless, it is imperative to conduct additional investigations in order to gain a comprehensive understanding of the fundamental mechanisms governing conductivity. Furthermore, it is crucial to refine and enhance the synthesis and characterization techniques employed for these nanoparticles in order to achieve optimal results.

The figure 18 illustrates the conductivity of three samples: ZnO nanoparticles (red), proteinoids (blue), and their mixture (green). The y-axis of the graph is measured in S cm^{-1} . The graph shows that a combination of proteinoids and colloidal ZnO nanoparticles has a higher conductivity than either component alone at all frequencies. ZnO and proteinoids may explain this since their combination creates a hybrid material with improved electrical features. ZnO nanoparticles may be more aligned and in better contact with one another thanks to the proteinoid's potential role as a binder or matrix. The ZnO nanoparticles' conductivity could be improved as a result of an increase in their effective surface area and charge transport. Due to its molecular structure and charge distribution, the proteinoid may also have some intrinsic conductivity, which could add to the mixture's overall conductivity. There may be a synergistic impact between ZnO and proteinoids that improves their electrical performance when used together [47, 48].

This section presents the results of using Lempel–Ziv complexity (LZC) and entropy rate (ER) metrics [49, 50] to analyse the complexity and information content of conductivity data from proteinoid-colloidal ZnO samples. In MATLAB, conductivity values are converted to binary sequences. The LZC and ER values are then estimated utilising the `calclzcomplexity` and `kolomogorov` functions. The LZC and ER values were calculated for three distinct time series, namely P (Proteinoid L-Glu:L-Arg), ZnO (Colloidal ZnO), and PZnO (the combination of Proteinoid-ZnO hybrid). The findings are presented in

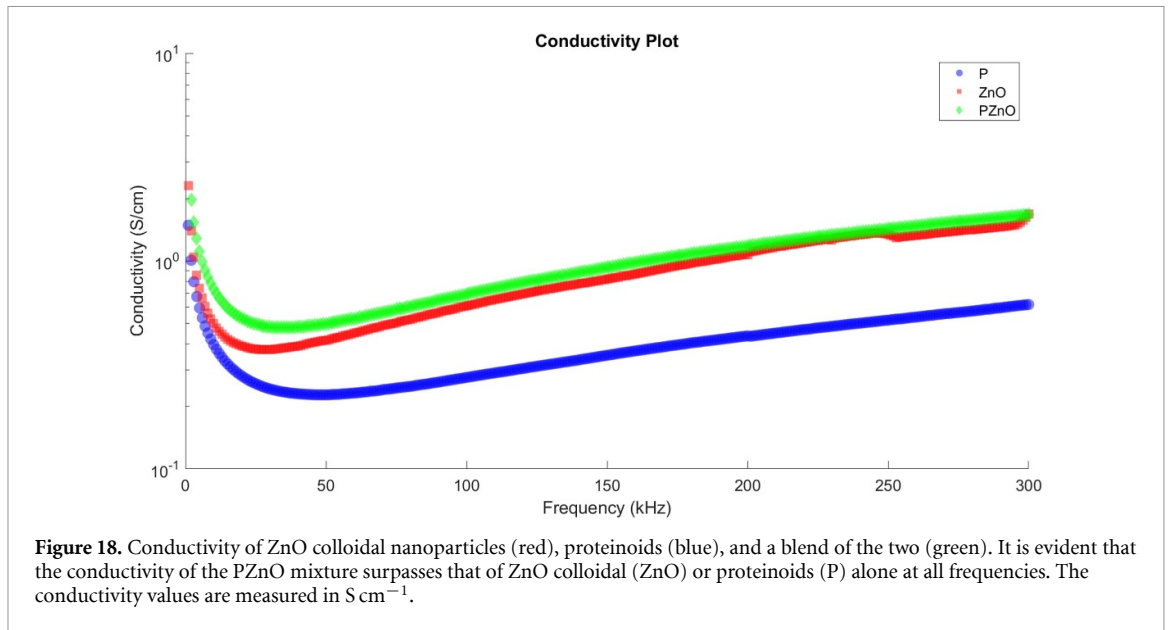


Table 7. LZ complexity and entropy rate values for various time series for P (Proteinoid L-Glu:L-Arg), ZnO (Colloidal ZnO Nanoparticles), and PZnO (the Proteinoid-ZnO NP hybrid).

Time series	LZ complexity	Entropy rate
P (Proteinoid L-Glu:L-Arg)	0.192 006	0.192 006
ZnO (Colloidal ZnO Nanoparticles)	0.356 582	0.192 006
PZnO (the mixture of Proteinoid-ZnO NP)	0.192 006	0.164 576

table 7. LZC values for P are 0.192 006, 0.356 582 for ZnO, and 0.192 006 for PZnO. The ERs for P are 0.192 006, ZnO is 0.192 006, and PZnO is 0.164 576. The ZnO time series exhibited the highest values for both LZC and ER, suggesting its superior complexity and informativeness. The P time series exhibited the highest regularity and predictability as evidenced by its lowest LZC and ER values. The PZnO time series had intermediate LZC and ER values, indicating that it was less complex and informative than ZnO but more complex and informative than P. The findings indicate that the combination of proteinoid and colloidal ZnO nanoparticles exhibits distinct complexity and information content compared to their individual constituents. Additionally, colloidal ZnO nanoparticles display a greater rate of generating novel patterns than proteinoid.

A common machine learning approach, decision trees can be used to solve both classification and regression issues. They can also be used in unconventional computing [51–53], which deviates from the standard von Neumann computer architecture to investigate new models and paradigms of processing data. One sort of unconventional computer that takes use of the nonlinear dynamics of chemical reactions is the proteinoids-ZnO colloid hybrid, whose electrical spiking properties can be analysed and optimised using decision trees [54]. Quantum systems, another type of unconventional computing that relies on quantum mechanical processes, can be modelled and simulated using decision trees [55]. There are many advantages to adopting decision trees, including low power consumption, high speed, and parallelism [56], and the fact that they can be implemented using unconventional technology like spintronics and optoelectronics. As a result, decision trees are an effective and flexible resource for novel uses of computing.

Based on the LZ complexity and ER values of the electrical spiking signals, we created a decision tree to explain how we selected the optimal time series for biological computing applications. The analytic hierarchy process technique [57] was used to build the decision tree depicted in figure 19; this technique allows us to compare alternatives on the basis of several criteria and give weights to each criterion based on their relative importance. Based on the weights assigned by the decision tree, LZ complexity is the primary factor, carrying a value of 0.833, followed by ER, which carries a value of 0.167. Each option's score and placement in the hierarchy are displayed in the decision tree based on how well it meets each criterion. The total score is arrived at by multiplying each criterion's score by its weight and adding the results together. The order is based on a descending ordering of the alternatives' final ratings. Based on the decision tree's weighting of each factor, PZnO comes out on top with a total score of 0.417, followed by P (0.381) and ZnO (0.201). As a result, we think PZnO is the best material for our needs.

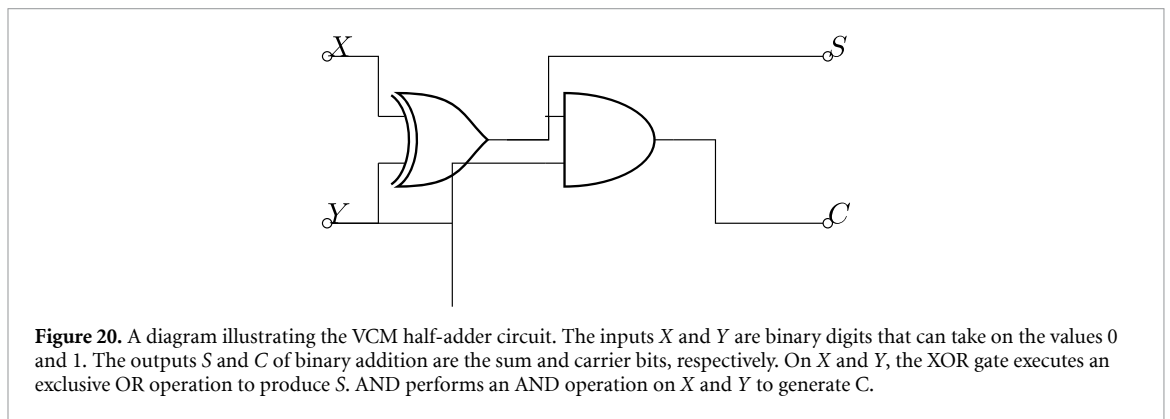
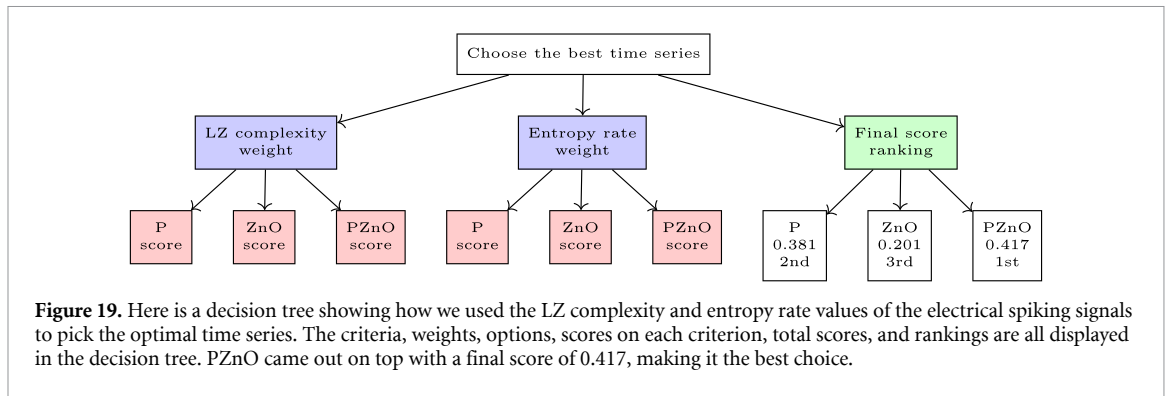


Table 8. Input-output table for the VCM half-adder circuit.

X	Y	Sum	Carry
-1	-1	0	1
-1	0	-1	0
-1	1	0	-1
0	-1	-1	0
0	0	0	0
0	1	1	0
1	-1	0	-1
1	0	1	0
1	1	0	1

The electrochemical activity exhibited by colloidal zinc oxide nanoparticles makes them highly suitable for the integration and utilisation within electronic devices, including but not limited to the half-adder. The nanoparticles exhibit electrochemical activity, which enables the generation and utilisation of electrical signals in diverse physical applications, such as logic gates. In addition, it is worth noting that the utilisation of nanoparticles is facilitated by their small dimensions, which enable the simple development of interconnections between the various inputs and outputs of the half-adder circuitry. Proteinoid nanoparticles, being derivatives of proteins, exhibit enhanced suitability for facilitating the required interconnections between inputs and outputs within the context of this particular application [58]. The VCM half-adder circuit performs binary addition, producing a sum and a carry. The significance of a VCM half-adder circuit in biological computing lies in its potential as a fundamental component for intricate arithmetic circuits, including full adders, multipliers, and dividers. The VCM half-adder circuit has the capability to execute various logic operations, including XOR and NIMPLY, through distinct arrangements of the sum and carry outputs. A VCM half-adder circuit (figure) 20 is a circuit that adds together two binary integers, producing a sum and a carry. Using the sign function, the table 8 identifies the input bits X and Y as the sign bits of the conductivities of proteinoids and zinc oxide nanoparticles. The sign function returns -1 when the input is negative, 0 when the input is zero, and 1 when the input is positive.

4. Discussion

This study investigates the electrical spiking characteristics of proteinoid-ZnO colloid hybrids, which consist of abiotically formed protein-like molecules from amino acids and zinc oxide nanoparticles. Proteinoids are considered potential antecedents of living cells and exhibit enzymatic properties. Zinc oxide is a semiconductor with a wide band gap and diverse applications in optics, electronics, catalysis, and sensing.

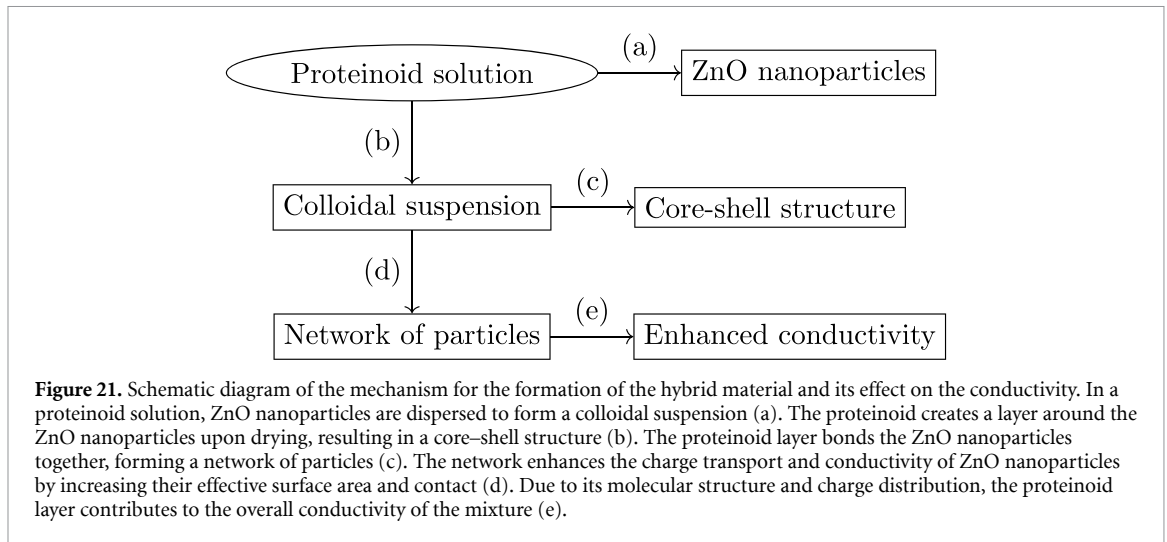
The occurrence of spiking behavior in proteinoids is most likely a result of electrochemical redox processes involving their constituent polypeptides. Reported conductive proteinoids consist predominantly of chains formed from various amino acid precursors polymerized into polypeptides, including formulations with non-redox active amino acids [1]. The produced proteinoids predominantly consist of polypeptide chains formed from polymerized L-glutamic acid and L-arginine, present in an equimolar ratio of 1:1 in the reacted amino acid mixture. While tyrosine and tryptophan amino acid side chains can contribute redox activity, proteinoid conductivity and excitability have been reported from various precursor formulations [8, 59]. When exploring complex interfacial dynamics that emerge between synthetic biological materials and inorganic substrates, it is critical to consider the thermodynamic forces at play. Our proteinoid-ZnO bilayer system demonstrating electrical excitability exists in an intrinsically non-equilibrium state facilitated by chemical potential gradients across the junction. The sustained voltage oscillations measured arise from the continuous shuttling of charge carriers and peptides between the phases. Input of chemical energy via ongoing hydrolysis further accentuates the departure from equilibrium. While self-organized spiking behaviors have been characterized under these conditions, quantifying the fluxes of energy and mass that perturb and maintain this dynamic proteinoid-inorganic hybrid away from equilibrium will offer deeper insight into the orchestration of its autonomous electrical activity from the standpoint of non-equilibrium thermodynamics. Furthermore, the PZnO composite facilitates electrochemical activity by charge transfer between the proteinoids and ZnO nanoparticles. UV irradiation of ZnO generates excited electrons that can engage in redox reactions with amino acids at the nano-bio interface. The synchronisation of spikes between samples may arise from the intrinsic electrical connectivity of the proteinoids through shared conformational substructures and peptide backbone components. The comparable chemical composition facilitates the coordinated movement of electric charges. Moreover, in the context of PZnO, the ZnO nanoparticles have the ability to facilitate the flow of electrons across proteinoids, resulting in synchronisation. The homogeneous distribution of nanoparticles in the composite allows for the formation of interconnected regions with a high electron affinity, facilitating electron delocalization.

The study demonstrates that the capacitance and frequency of proteinoid-ZnO colloid hybrids exhibit a significant enhancement in comparison to the separate constituents. The capacitance and frequency limits for the mixture are 535 μF and 1.02 kHz, respectively. In comparison, the proteinoid and zinc oxide nanoparticles have maximum capacitance and frequency values of 4.7530 μF and 1.02 kHz, respectively. The mixture has a minimum capacitance of 0.0032 μF and a minimum frequency of 300 kHz. The proteinoid and zinc oxide nanoparticles have minimum capacitances of 0.0086 μF and minimum frequencies of 0.02 kHz, respectively.

At all frequencies, the mixture of ZnO and proteinoid had a higher conductivity than ZnO colloid and proteinoid alone. This could be the result of the fabrication of a hybrid material with improved electrical properties. The proteinoid may function as a matrix or binder that holds the ZnO nanoparticles together and enhances their alignment and contact. This may increase the ZnO nanoparticles' effective surface area and charge transport, resulting in greater conductivity. Due to its molecular structure and charge distribution, the proteinoid may have some intrinsic conductivity, which may contribute to the overall conductivity of the mixture. There may be a synergistic effect between ZnO and proteinoid that improves the electrical efficacy of both components. Figure 21 depicts a possible mechanism for the formation of the hybrid material and its influence on the conductivity.

The findings indicate a significant correlation between proteinoid and zinc oxide nanoparticles, resulting in improved electrical characteristics. The study suggests that metal ions, specifically zinc and copper, serve as catalysts or co-factors for proteinoid enzyme activities in this interaction. The study proposes that proteinoid-ZnO colloid hybrids exhibit potential utility in bioelectronics, biosensors, biocatalysis, and artificial cells.

The study findings indicate that the electrical spiking properties of proteinoids-ZnO colloid hybrids are superior to those of pure proteinoids and pure ZnO nanoparticles. The enhanced electrical conductivity, optical transparency, photostability, and photocatalytic ability of the hybrids may be attributed to the synergistic effects of proteinoids and ZnO nanoparticles [42, 58]. Proteinoids serve as a biocompatible and self-assembling matrix for ZnO nanoparticles, which in turn improve the electrical and optical properties of



the proteinoids. The spiking response of proteinoids-ZnO hybrids can be adjusted by varying the ratio of proteinoids and ZnO nanoparticles, as well as the size, shape, chemical composition, and surface morphology of the ZnO nanoparticles [58]. The proteinoids-ZnO colloid hybrids exhibit potential as innovative bioinspired materials for use in organic and hybrid optoelectronic devices, as demonstrated by our study. Proteinoids-ZnO hybrids have potential applications as n-type buffer layers for polymer solar cells [60], as well as in neuromorphic computing for sensors, actuators, transistors, and memristors. Proteinoids-ZnO hybrids offer potential benefits compared to traditional metal oxide or polymer materials due to their biocompatibility, biodegradability, low toxicity, low cost, and easy synthesis. Additional research is required to enhance the production and analysis of proteinoids-ZnO hybrids, and to investigate their operational efficiency and durability in diverse environmental settings.

This study examines the electrical spiking properties of proteinoids-ZnO colloid hybrids (PZnO) in response to various stimuli. PZnO display nonlinear and chaotic characteristics similar to those of biological neurons. The complexity and information content of the conductivity data of PZnO were analysed using LZC and ER metrics to comprehend the fundamental mechanisms of these behaviours. LZC and ER are metrics used to assess the randomness and indeterminacy of a binary sequence obtained from a temporal dataset. Greater LZC and ER values indicate greater irregularity and complexity in time series. Lower LZC and ER values indicate greater regularity and simplicity in time series. These metrics are utilised to characterise signal complexity in various domains, including EEG, ECG, speech, and music [61–63]. Table 7 displays the LZ complexity and ER values of various time series. These measures assess the level of randomness and predictability of the electrical spiking signals produced by the hybrids of proteinoids and ZnO colloids. The table indicates that ZnO nanoparticles exhibit higher LZ complexity compared to proteinoids and their mixture, implying that ZnO nanoparticles generate more intricate and erratic signals. The mixture exhibits a higher degree of order and regularity in its spiking patterns compared to proteinoids and ZnO nanoparticles, as evidenced by its lower ER. The study shows that the electrical spiking properties of proteinoids-ZnO colloid hybrids are composition and interaction-dependent.

Unlike individual device mimics of neural components, our proteinoid-ZnO bilayers integrate an artificial biological phase with an inorganic substrate, approximating the multifaceted emergent dynamics at native synapses. Unlike synthetic biology biomaterials, proteinoids offer simpler abiotic models balancing biological inspiration with custom-designed functionalities. Their biocompatibility also enables direct bio-interfacing for modulation of living tissue activity. While other platforms may better replicate singular neural behaviours [64], the proteinoid-ZnO hybrid's configurational richness elicits versatile spike patterns with bidirectional bio-coupling potential.

Bioelectronics is a new discipline that attempts to combine biological materials with electronic ones for use in fields including sensing, computing, communication, and medicine [65]. Our research is a part of this growing field. Proteinoid-ZnO colloid hybrids have potential benefits for bioelectronic applications due to their biocompatibility, biodegradability, self-assembly, enzyme-like activity, electrical spiking behaviour, and adjustable properties based on component composition and ratio. Proteinoid-ZnO colloid hybrids have potential applications as artificial synapses or neurons that emulate the electrical signalling of biological cells. They have potential applications as biosensors for detecting changes in environmental conditions or biomolecules through capacitance or frequency responses.

The proteinoids–ZnO colloids display pronounced electrical activity spikes, indicating their potential usefulness in neuromorphic computing systems [66, 67] aimed at emulating biological neural networks [68]. Nevertheless, the achievement of understanding in these bioinspired systems necessitates more theoretical assessment. Colloids have the ability to act as integrate–and–fire neurons, where the voltage dynamics they exhibit can represent the membrane potential. Modelling studies are necessary to ascertain the exact amplitude and duration of stimulation needed to induce spiking oscillations. The voltage thresholds must align with the established parameters of current neuromorphic technology [69], which typically operates within the range of 0–10 mV. Evaluation of the proteinoids–ZnO colloids as artificial spiking neurons can be guided by literature data for neuron membrane potentials and action potential production. An analysis of spike amplitude, duration, rise and fall timings, firing patterns, and noise can help identify the most favourable formulations for neuromorphic networks. In order to accurately replicate synaptic connections, the colloids must exhibit plasticity in spike transmission, such as through spike timing or frequency dependent learning principles. Additional research is necessary to comprehend the potential of proteinoids–ZnO composites in imitating synaptic weight alterations and memory. Furthermore, it is necessary to assess the compatibility of complementary metal–oxide–semiconductor (CMOS) by comparing the synthesis methods of ZnO and proteinoids with well–established CMOS fabrication techniques [70]. The modular colloid technique [71, 72] is very suitable for microelectronic integration, however it may necessitate process optimisations. To summarise, although the dynamic electrical activity shows promise, extensive modelling, characterisation, and materials development are required to thoroughly evaluate the appropriateness of proteinoids–ZnO for bioinspired computing. We suggest that this future research can clarify their potential in neuromorphic computing systems.

The current work provides initial insights into the electrical characteristics of proteinoid–ZnO composites. However, there are still many unanswered questions that need to be addressed in future in–depth studies. Areas that could be further explored include studying the effects of environmental factors like pH, temperature, and ionic strength on electrochemical activity. Advanced spectroscopic techniques could be used to investigate interactions between proteinoids and nanoparticles, revealing information about band structure and electron transfer kinetics. The role of surface chemistry in electrical coupling could also be examined, as well as the impact of proteinoid composition and conformation on electrical behaviours. Understanding the biophysical mechanisms of long–range electron conduction along proteinoids is another area of interest. Additionally, developing new metrics and models to describe the dynamics and information processing capabilities of these adaptive, self–assembled electrically active composites would be valuable. Through a careful investigation of these areas, it is possible to discover new design principles for developing functional bio–inorganic materials that effectively combine the electrical properties of proteinoids and semiconducting nanoparticles. The current study presents initial findings and proposed mechanisms, highlighting the need for further interdisciplinary research to fully explore the capabilities of proteinoid–nanoparticle bioelectronic systems. Furthermore, it may be interesting to investigate whether the irregular voltage patterns displayed by the proteinoid–ZnO composites exhibit chaotic dynamics. The utilisation of methods like computing the largest Lyapunov exponent could provide insights into whether the intricate and irregular patterns are indicative of an underlying chaotic system [73–75]. The electrical activity’s chaotic features offer valuable insights into the complex mechanisms that occur at the nano–bio interface. Chaos can provide valuable insights into predicting future behaviour by analysing initial conditions. Additional extensive analysis of the voltage fluctuations in the proteinoid–ZnO colloidal nanoparticle composites could reveal intriguing insights into their self–organizing nature.

5. Conclusion

We investigated the electrical spiking properties of hybrids consisting of proteinoids and ZnO colloids. Proteinoids were synthesised through thermal polymerization of amino acids and subsequently combined with ZnO nanoparticles to create a composite colloid. The electrical activity of the colloid was assessed under varying electrical stimulation conditions and the spiking patterns were analysed. We uncovered the following phenomena. Similar to proteinoids alone, the proteinoids–ZnO colloid exhibited endogenous electrical charging. The colloid’s spiking characteristics are influenced by the electrical stimulation’s frequency and voltage, specifically in terms of amplitude, period, and pattern. The addition of ZnO colloid to proteinoid mixture resulted in increased sensitivity and quicker response to electrical stimulation compared to proteinoids in isolation. ZnO nanoparticles improved the electrical sensing performance of the colloid by enhancing electron transport and extraction. The study indicates that proteinoids–ZnO colloid hybrids possess the capability to be utilised as electrical sensors and, potentially, unconventional computing devices. Future research will aim to optimise the synthesis and characterisation of the colloid, and investigate its interactions with other stimuli and substrates.

Data availability statement

The raw data can be found in the supplementary files. The data that support the findings of this study are available upon reasonable request from the authors.

Acknowledgments

P M and A A were supported by EPSRC Grant EP/W010887/1 'Computing with proteinoids'. Authors are grateful to David Paton for helping with SEM imaging and to Neil Phillips for helping with instruments. N R H and A C received a support from the European Innovation Council and SMEs Executive Agency (EISMEA) under Grant Agreement No. 964388.

ORCID iDs

Panagiotis Mougkogiannis  <https://orcid.org/0000-0003-1710-4917>

Alessandro Chiolerio  <https://orcid.org/0000-0001-9328-2999>

References

- [1] Fox S W 1992 Thermal proteins in the first life and in the "mind-body" problem *Evolution of Information Processing Systems* (Springer) pp 203–28
- [2] Harada K and Fox S W 1958 The thermal condensation of glutamic acid and glycine to linear peptides1 *J. Am. Chem. Soc.* **80** 2694–7
- [3] Dose K 1974 Chemical and catalytical properties of thermal polymers of amino acids (proteinoids) *Orig. Life* **5** 239–52
- [4] Mita H, Kuwahara Y and Nomoto S 2010 Chemical and physical structures of proteinoids and related polyamino acids *38th COSPAR Scientific Assembly* vol 38 p 4
- [5] Telegina T, Masinovsky Z, Sivash A, Pavlovskaya T, Liebl V and Bejšovcová L 1990 Proteinoids as complexes of polyamino acids with melanoidins *Orig. Life Evol. Biosph.* **20** 269–77
- [6] Follmann H 1982 Deoxyribonucleotide synthesis and the emergence of dna in molecular evolution *Naturwissenschaften* **69** 75–81
- [7] Van Gestel J and Tarnita C E 2017 On the origin of biological construction, with a focus on multicellularity *Proc. Natl Acad. Sci.* **114** 11018–26
- [8] Przybylski A T 1985 Excitable cell made of thermal proteinoids *BioSystems* **17** 281–8
- [9] Mougkogiannis P, Phillips N and Adamatzky A 2023 Transfer functions of proteinoid microspheres *Biosystems* **227** 104892
- [10] Sasson E, Pinhasi R V O, Margel S and Klipcan L 2020 Engineering and use of proteinoid polymers and nanocapsules containing agrochemicals *Sci. Rep.* **10** 1–13
- [11] Meng Y et al 2021 Optical meta-waveguides for integrated photonics and beyond *Light Sci. Appl.* **10** 235
- [12] Naghdi T, Golmohammadi H, Yousefi H, Hosseinifard M, Kostiv U, Horak D and Merkoci A 2020 Chitin nanofiber paper toward optical (bio) sensing applications *ACS Appl. Mater. Interfaces* **12** 15538–52
- [13] Hmar J J L 2018 Flexible resistive switching bistable memory devices using ZnO nanoparticles embedded in polyvinyl alcohol (PVA) matrix and poly (3, 4-ethylenedioxythiophene) polystyrene sulfonate (PEDOT: PSS) *RSC Adv.* **8** 20423–33
- [14] Barnes B K and Das K S 2018 Resistance switching and memristive hysteresis in visible-light-activated adsorbed ZnO thin films *Sci. Rep.* **8** 2184
- [15] Muhammad N M, Duraisamy N, Rahman K, Dang H W, Jo J and Choi K H 2013 Fabrication of printed memory device having zinc-oxide active nano-layer and investigation of resistive switching *Curr. Appl. Phys.* **13** 90–96
- [16] Chiolerio A, Roppolo I, Bejtka K, Asvarov A and Pirri C F 2016 Resistive hysteresis in flexible nanocomposites and colloidal suspensions: interfacial coupling mechanism unveiled *RSC Adv.* **6** 56661–7
- [17] Kheirabadi N R, Chiolerio A, Phillips N and Adamatzky A 2022 Learning in colloids: Synapse-like ZnO+ DMSO colloid (arXiv:2211.00419)
- [18] Kheirabadi N R, Chiolerio A and Adamatzky A 2022 Pavlovian reflex in colloids (arXiv:2211.06699)
- [19] Matsuno K 1984 Electrical excitability of proteinoid microspheres composed of basic and acidic proteinoids *BioSystems* **17** 11–14
- [20] Stratten W P 1984 Protocell action potentials: a new perspective of bio-excitation *Molecular Evolution and Protobiology* (Springer) pp 233–51
- [21] Matveev V V 2019 Cell theory, intrinsically disordered proteins and the physics of the origin of life *Prog. Biophys. Mol. Biol.* **149** 114–30
- [22] Chiolerio A and Quadrelli M B 2017 Smart fluid systems: the advent of autonomous liquid robotics *Adv. Sci.* **4** 1700036
- [23] Hu G, An H, Xi J, Lu J, Hua Q and Peng Z 2021 A ZnO micro/nanowire-based photonic synapse with piezo-phototronic modulation *Nano Energy* **89** 106282
- [24] Zhang Z-Y and Xiong H-M 2015 Photoluminescent ZnO nanoparticles and their biological applications *Materials* **8** 3101–27
- [25] Kahn A 2016 Fermi level, work function and vacuum level *Mater. Horiz.* **3** 7–10
- [26] Giridharagopal R and Ginger D S 2010 Characterizing morphology in bulk heterojunction organic photovoltaic systems *J. Phys. Chem. Lett.* **1** 1160–9
- [27] Shao G, Rayermann G E, Smith E M and Ginger D S 2013 Morphology-dependent trap formation in bulk heterojunction photodiodes *J. Phys. Chem. B* **117** 4654–60
- [28] Nouiri M, Guefreche A, Djessas K and L 2020 El Mir, Highlighting the Au/TiO₂ role in the memory effect of Au/TiO₂/TiO₂/ZnO: Al/p-si heterostructure *J. Mater. Sci.: Mater. Electron.* **31** 7084–92
- [29] Kwiatkowski M, Bezverkhy I and Skompska M 2015 ZnO nanorods covered with a TiO₂ layer: simple sol-gel preparation and optical, photocatalytic and photoelectrochemical properties *J. Mater. Chem. A* **3** 12748–60
- [30] Kreuz T, Mulansky M and Bozanic N 2015 Spiky: a graphical user interface for monitoring spike train synchrony *J. Neurophysiol.* **113** 3432–45

- [31] Unakafova V A and Gail A 2019 Comparing open-source toolboxes for processing and analysis of spike and local field potentials data *Front. Neuroinf.* **13** 57
- [32] Mulansky M, Bozanic N, Sburlea A and Kreuz T 2015 A guide to time-resolved and parameter-free measures of spike train synchrony 2015 *Int. Conf. on Event-Based Control, Communication and Signal Processing (EBCCSP)* (IEEE) pp 1–8
- [33] Gu C, Cheng C, Huang H, Wong T, Wang N and Zhang T-Y 2009 Growth and photocatalytic activity of dendrite-like ZnO@ ag heterostructure nanocrystals *Cryst. Growth Des.* **9** 3278–85
- [34] Nadupalli S, Repp S, Weber S and Erdem E 2021 About defect phenomena in ZnO nanocrystals *Nanoscale* **13** 9160–71
- [35] Zeng H, Liu P, Cai W, Yang S and Xu X 2008 Controllable pt/ZnO porous nanocages with improved photocatalytic activity *J. Phys. Chem. C* **112** 19620–4
- [36] Fox S W and Dose K 1972 Molecular evolution and the origin of life (available at: <https://cir.nii.ac.jp/crid/1130000798120497024>)
- [37] Fox S W and Harada K 1958 Thermal copolymerization of amino acids to a product resembling protein *Science* **128** 1214–1214
- [38] Laurenti M, Verna A and Chiolerio A 2015 Evidence of negative capacitance in piezoelectric ZnO thin films sputtered on interdigital electrodes *ACS Appl. Mater. Interfaces* **7** 24470–9
- [39] Phetcharee K, Pholauyphon W, Kwamman T, Sirisit N, Manyam J and Paoprasert P 2023 Enhancing specific capacitance and cycling stability of zinc oxide-based supercapacitors using gamma-irradiated, amine-passivated carbon dots *J. Alloys Compd.* **933** 167631
- [40] Yan B, Zheng J, Wang F, Zhao L, Zhang Q, Xu W and He S 2021 Review on porous carbon materials engineered by ZnO templates: design, synthesis and capacitance performance *Mater. Design* **201** 109518
- [41] Rani N, Saini M, Yadav S, Gupta K, Saini K and Khanuja M 2020 High performance super-capacitor based on rod shaped ZnO nanostructure electrode *AIP Conf. Proc.* **2276** 020042
- [42] Lee W et al 2020 High colloidal stability ZnO nanoparticles independent on solvent polarity and their application in polymer solar cells *Sci. Rep.* **10** 1–10
- [43] Zhao S, Mehta A S and Zhao M 2020 Biomedical applications of electrical stimulation *Cell. Mol. Life Sci.* **77** 2681–99
- [44] Raha S and Ahmaruzzaman M 2022 ZnO nanostructured materials and their potential applications: progress, challenges and perspectives *Nanoscale Adv.* **4** 1868–925
- [45] Grove T, Masters M and Miers R 2005 Determining dielectric constants using a parallel plate capacitor *Am. J. Phys.* **73** 52–56
- [46] Korcala A, Plóciennik P, Lougdali M and Anoua R 2019 Admittance spectroscopy of organic and metal-organic complexes 2019 *21st Int. Conf. on Transparent Optical Networks (ICTON)* (IEEE) pp 1–3
- [47] Zhang W, Chen X, Wang Y, Wu L and Hu Y 2020 Experimental and modeling of conductivity for electrolyte solution systems *ACS Omega* **5** 22465–74
- [48] Vadhma P, Hu J, Johnson M J, Stocker R, Braglia M, Brett D J and Rettie A J 2021 Electrochemical impedance spectroscopy for all-solid-state batteries: theory, methods and future outlook *ChemElectroChem* **8** 1930–47
- [49] Restrepo J E, Mateos D M and Schlotthauer G 2020 Transfer entropy rate through lempel-ziv complexity *Phys. Rev. E* **101** 052117
- [50] Amigó J M, Szczepański J, Wajnryb E and Sanchez-Vives M V 2004 Estimating the entropy rate of spike trains via lempel-ziv complexity *Neural Comput.* **16** 717–36
- [51] Adamatzky A, Bull L and Costello B D L 2007 *Unconventional Computing 2007* (Luniver Press)
- [52] Li S, Kang W, Zhang X, Nie T, Zhou Y, Wang K L and Zhao W 2021 Magnetic skyrmions for unconventional computing *Mater. Horiz.* **8** 854–68
- [53] Adamatzky A et al 2017 East-west paths to unconventional computing *Prog. Biophys. Mol. Biol.* **131** 469–93
- [54] Tayur S 2021 Unconventional computing: applications, hardware, algorithms (available at: www.cmu.edu/tepper/news/stories/2021/february/quantum-computing-tayur.html)
- [55] Thomas T, Vijayaraghavan A P, Emmanuel S, Thomas T, Vijayaraghavan A P and Emmanuel S 2020 Applications of decision trees *Machine Learning Approaches in Cyber Security Analytics* pp 157–84
- [56] Mayne R 2016 *Orchestrated Biocomputation: Unravelling the Mystery of Slime Mould Intelligence* (Luniver Press)
- [57] Vaidya O S and Kumar S 2006 Analytic hierarchy process: an overview of applications *Eur. J. Oper. Res.* **169** 1–29
- [58] van Embden J, Gross S, Kittilstved K R and Della Gaspera E 2022 Colloidal approaches to zinc oxide nanocrystals *Chem. Rev.* **123** 271–326
- [59] Ishima Y, Przybylski A T and Fox S W 1981 Electrical membrane phenomena in spherules from proteinoid and lecithin *BioSystems* **13** 243–51
- [60] Wang Z, Bockstaller M R and Matyjaszewski K 2021 Synthesis and applications of ZnO/polymer nanohybrids *ACS Mater. Lett.* **3** 599–621
- [61] Lempel A and Ziv J 1976 On the complexity of finite sequences *IEEE Trans. Inf. Theory* **22** 75–81
- [62] Li Y, Geng B and Jiao S 2022 Dispersion entropy-based lempel-ziv complexity: a new metric for signal analysis *Chaos, Solitons Fractals* **161** 112400
- [63] Nalewajski R F 2006 *Information Theory of Molecular Systems* (Elsevier)
- [64] Przychyna D, Zawal P, Mazur T, Strzelecki M, Gentili P L and Szaciłowski K 2020 In-materio neuromimetic devices: Dynamics, information processing and pattern recognition *Jpn. J. Appl. Phys.* **59** 050504
- [65] Rashid R B, Du W, Griggs S, Maria I P, McCulloch I and Rivnay J 2021 Ambipolar inverters based on cofacial vertical organic electrochemical transistor pairs for biosignal amplification *Sci. Adv.* **7** eabh1055
- [66] Furber S 2016 Large-scale neuromorphic computing systems *J. Neural Eng.* **13** 051001
- [67] Calimera A, Macii E and Poncino M 2013 The human brain project and neuromorphic computing *Funct. Neurol.* **28** 191
- [68] Eluyode O and Akomolafe D T 2013 Comparative study of biological and artificial neural networks *Eur. J. Appl. Eng. Sci. Res.* **2** 36–46
- [69] Bartolozzi C, Indiveri G and Donati E 2022 Embodied neuromorphic intelligence *Nat. Commun.* **13** 1024
- [70] Radamson H H et al 2020 State of the art and future perspectives in advanced cmos technology *Nanomaterials* **10** 1555
- [71] Bollhorst T, Rezwan K and Maas M 2017 Colloidal capsules: nano- and microcapsules with colloidal particle shells *Chem. Soc. Rev.* **46** 2091–126
- [72] Xie B, Parkhill R L, Warren W L and Smay J E 2006 Direct writing of three-dimensional polymer scaffolds using colloidal gels *Adv. Funct. Mater.* **16** 1685–93
- [73] Dong Y, Yang S, Liang Y and Wang G 2022 Neuromorphic dynamics near the edge of chaos in memristive neurons *Chaos, Solitons Fractals* **160** 112241
- [74] Pathak J, Lu Z, Hunt B R, Girvan M and Ott E 2017 Using machine learning to replicate chaotic attractors and calculate lyapunov exponents from data *Chaos* **27** 121102
- [75] Hochstetter J, Zhu R, Loeffler A Diaz-Alvarez A, Nakayama T and Kuncic Z 2021 Avalanches and edge-of-chaos learning in neuromorphic nanowire networks *Nat. Commun.* **12** 4008